Electrochemical Generation of Ruthenium (IV)–oxo Complexes: An Unexpected Promotion Effects from the Alkyl-tailed Ligand and Anions

Chui-Shan Tsang, Lawrence Yoon Suk Lee, Kwong-Chak Cheung, Zhong-Yuan Zhou, Wing-Leung Wong, and Kwok-Yin Wong*

Department of Applied Biology and Chemical Technology and the State Key Laboratory of Chemical Biology and Drug Discovery, The Hong Kong Polytechnic University, Hung Hom, Kowloon, Hong Kong SAR

ABSTRACT: Promotion of the electro-generation of Ru^{IV}=O species from Ru−aqua complex is crucial to facilitate the performance in electrocatalytic water oxidation. Up to date, there is still lack of Ru-complex that is able to enhance the conversion of Ru^{III}–OH to Ru^{IV}=O couple effectively. We report herein a new series of alkyl-tailed Ru^{II}-aqua complexes, $[Ru(tpy)(\mathbf{L})(OH_2)]^{2+}$, of *N*-substituted 2,2′-dipyridylamine ligands tagged with alkyl chain **L** (**L** = **dppa**: 2,2'-dipyridyl-*n*-propylamine, **dpha**: 2,2'-dipyridyl-*n*-hexylamine, **dpoa**: 2,2'-dipyridyl-*n*-octylamine) with *X*-ray crystal structural characterizations. The length of the alkyl chain substituted dipyridylamine ligand exerted a great influence in enhancing the *in situ* electro-generation of Ru^{IV}=O species. Electrochemical study of these complexes in 0.01 M CF_3SO_3H aqueous solution (pH = 2, I = 0.1 M) shows that **L** of a longer alkyl chain promotes a much better-defined Ru^{III}–OH to Ru^{IV}=O couple. Moreover, the couple can be further enhanced by the addition of perchlorate anions. Chronocoulometric studies suggest that the promoted generation of $Ru^{III/IV}$ couple is originated from the adsorption of the complexes onto glassy carbon working electrode surface. With the boosted generation of Ru(IV)–oxo species, the electrocatalytic activity of the Ru^{II}-aqua complexes for water oxidation was investigated. Among the complexes, $[Ru(tpy)(\mathbf{dppa})(OH_2)]^{2+}$ was found to be the most active one in the bulk electrolysis.

INTRODUCTION

Proton-coupled electron transfer (PCET) process plays a vital role in numerous biological processes in nature, such as photosynthesis and respiration[1-10] and its emerging applications have recently been demonstrated in some important chemical processes including renewable energy developments, particularly water splitting and carbon dioxide reduction.[11-14] The mechanism of PCET that involving a simultaneous transfer of protons and electrons is known as a stepwise or concerted process depending on the stability of the reaction intermediates.[11, 15] PCET is observed commonly in certain transition metal–aqua complexes ($M^{II}–OH_2$) and is enhanced by increasing the acidity of aqueous media. The sequential oxidation *via* the loss of a proton in the complex within a relatively narrow potential range generates high-valent metal species (M^{III}–OH and M^{IV}=O), which are the active intermediates in various electrocatalytic reactions such as water oxidation.[16-22] To realize of the utilization of metal oxo-complexes in energy conversion and catalysis through the PCET process[12, 23-30], researchers are continuously to develop high-valent metal oxo-complexes with high stability and catalytic activity.

Metal-catalyzed water oxidations have been extensively studied over the past decades and the polypyridyl ruthenium aqua complexes are found the most used catalysts probably due to their robustness and high catalytic activity.[17, 31-34] Nowadays, the Ru^{IV}=O complex is identified as the key intermediate in water oxidation,[35-41] however, the oft-cited kinetically distorted electrochemical interconversions between Ru^{III}–OH and Ru^{IV}=O have not yet been fully understood. In addition, the formation of $Ru^{III/IV}$ redox couple in cyclic voltammetric experiments compared to its corresponding $Ru^{II/III}$ is commonly less favorable.[37, 42-44] Although it is generally accepted that the slow heterogeneous electron-transfer kinetics from solution to electrode surface is responsible for the lower intensity of $Ru^{III/IV}$ redox couple, the instability of

the high oxidation state intermediates in aqueous media could also be a possible factor. Therefore, it is very important to facilitate the Ru^{IV}=O species formation and, at the same time, to stabilize them through the coordination with suitable ligands.[32] Currently, the methods to accelerate the electro-generation of Ru^{IV}=O species are limited to electrochemical oxidation at an oxidatively pre-treated glassy carbon (GC) electrodes,[36] edge plane pyrolytic graphite electrodes (EPG),[45] GC electrodes with adsorbed quinones,[46] and immobilization of Ru-complexes onto an electro-conducting surface[47-58].

The electrochemical interconversion between Ru^{III}–OH and Ru^{IV}=O redox couples can be feasibly promoted with the coordination environment made of polypyridine ligands that are structurally stable towards hydrolysis and tolerate harsh oxidation conditions.[16-22] We speculated that the enhancement of Ru^{IV}=O species formation could also associate with the interaction property of the coordinated ligands with the electrode surface. However, there is no systematic study can be found in literature. Therefore, by developing a new pyridyl ligand system that can enhance the surface interactions, we can study their ability to promote Ru^{IV}=O species formation and also understand further the relationship between the complex-surface interaction and the generation of Ru^{IV}=O species. We herein reported a new series of alkyl-tailed Ru^{II}-aqua complexes, which were synthesized with *N*-alkyl-substituted 2,2′-dipyridylamine ligands (**dppa** = (2,2′-dipyridyl)-*n*-propylamine, **dpha** = 2,2′-dipyridyl-*n*-hexylamine, and **dpoa** = 2,2′-dipyridyl-*n*-octylamine). The electrochemical study of these complexes shows significant enhancement of electro-generation of Ru^{IV}=O species on a glassy carbon electrode (GCE) indicated by the experimental observation of the reversible Ru^{III}–OH and Ru^{IV}=O redox couple. In addition, the electrocatalytic activity of the Ru^{II}-aqua complexes in water oxidation was investigated.

EXPERIMENTAL SECTION

General information. All materials used are reagent grade and were used as received unless otherwise specified. Ruthenium(III) chloride trihydrate (ReagentPlus®), 2,2′:6′,2″-terpyridine (tpy) (98%), triethylamine (> 99%), lithium trifluoromethanesulfonate ($Li(CF_3SO_3)$) (99.995%, metals basis), silver trifluoromethanesulfonate (99%), trifluoromethanesulfonic acid (CF_3SO_3H) (98%), potassium hydroxide (> 90%, flakes), 2,2′-dipyridylamine (**dpa**) (99%), iodopropane (99%), iodohexane (> 98%), iodooctane (> 98%) and magnesium sulfate (> 99.5%, anhydrous) were purchased from Sigma-Aldrich. Lithium chloride (99%) and zinc powder were purchased from Thermo Fisher Scientific Inc. and BDH respectively. $[Ru(tpy)Cl_3]$ was synthesized according to literature reported procedure.[59] ^1H and ^{13}C NMR and ^1H–^1H correlation spectra were recorded on a Bruker ADVANCE III 400 or 600 MHz FT-NMR spectrometer at room temperature in $CDCl_3$ or D_2O with tetramethylsilane (TMS) as internal standard. Electrospray ionization mass spectra were recorded on a Finnigan Electrospray Ionization Mass Spectrometer (MAT 95) and the ACQUITY SQD MS system with Waters SQ Detector. Elemental analyses were performed by M-H-W Laboratories at Phoenix, Arizona in USA.

Electrochemical studies. Cyclic voltammetry (CV), differential pulse voltammetry (DPV), and chronocoulometry were performed on a Bioanalytical Systems (BAS) model 100W potentiostat or a CH Instruments model CHI1030A electrochemical analyzer at room temperature. Rotating disk voltammetry was performed on a Pine Instrument Company model AFMSRXE analytical rotator coupled with the potentiostats aforementioned. A conventional two-compartment cell with a sintered glass disc separating the two compartments was used. A glassy carbon (GC) electrode of area 0.07 cm^2 (BAS M2070), a platinum wire, and a saturated calomel electrode (SCE) were used as the working electrode, counter electrode, and reference electrode,

respectively. The working electrode was polished sequentially with 0.1 and 0.05 mm alumina (Buehler) on a micro-cloth. After rinsed with deionized water, the electrode was sonicated for 5 min in deionized water before use. Chronocoulometric measurements of the Ru^{II} aqua complexes, $[Ru(tpy)(\kappa^2\text{-N,N-}\mathbf{dpa})(OH_2)]^{2+}$, $[\mathbf{1b}]^{2+}$ and $[\mathbf{2b}]^{2+}$, were performed in 0.01 M CF_3SO_3H aqueous solution (pH = 2, I = 0.1 M) with the pulse width of 100 ms. The forward scans from chronocoulometric measurements were analyzed for adsorption in this study. The half-wave potentials ($E_{1/2}$) were estimated by averaging the anodic and cathodic peak potentials from cyclic voltammograms.

Electrochemical water oxidation. Bulk electrolysis was performed with a Princeton Applied Research Potentiostat model 273 A with reticular vitreous carbon (0.65 cm^3, S = 14.5 cm^2, 60 ppi) as working electrode. The reference electrode was an aqueous SCE electrode, and the counter electrode was a platinum gaze. The volume of the electrolyte, 1 M HOAc/NaOAc buffer (pH = 5.0), containing Ru^{II} aqua complex (0.075 mM) was 30 mL and the solution was purged with N_2 for 30 min prior to electrolysis. Oxygen that was generated in the headspace was analyzed by GC/TCD (Aligent 7890 A) fitted with an Agilent molecular sieve 5 Å plot column (30 m × 0.53 mm) with helium as carrier gas. Oxygen calibration curve was obtained by filling various amount of pure oxygen gas to a 500 mL flask with a graduated gastight syringe.

Synthesis of *N*,*N*-(di-2-pyridyl)-propylamine (dppa). 2,2′-Dipyridylamine (0.69 g, 4 mmol) was added to a suspension of potassium hydroxide (1.00 g, 18 mmol) in 10 mL of DMSO. The mixture was stirred at room temperature for 45 min. After addition of iodopropane (0.39 mL, 4 mmol), the reaction mixture was stirred for further 15 h. The reaction was quenched by addition of water (50 mL), and was extracted with diethyl ether for three times (3 × 50 mL). The collected organic extract was dried with magnesium sulfate and filtered. Solvent of the filtrate was

removed under reduced pressure to afford crude yellow oil which was purified with flash column chromatography (SiO_2) using petroleum ether/ethyl acetate (15:1) as eluent. White solids were obtained after removing solvent under reduced pressure. Yield: 0.60 g (70%). ^{1}H NMR (400 MHz, $CDCl_3$): δ 0.93 (t, 3H, *J* = 7.4 Hz), 1.72 (m, 2H), 4.13 (t, 2H, *J* = 7.7 Hz), 6.83 (t, 2H, *J* = 5.1 Hz), 7.08 (d, 2H, *J* = 8.4 Hz), 7.51 (t, 2H, *J* = 6.7 Hz), 8.33 (d, 2H, *J* = 4.9 Hz). ^{13}C NMR (100 MHz, $CDCl_3$): δ 11.58, 21.63, 50.15, 114.91, 116.96, 137.20, 148.47, 157.76. ESI-MS: *m/z* 214 $(M+H)^+$. Elemental analysis calc. for $C_{13}H_{15}N_3$: C, 73.2; H, 7.1; N, 19.7. Found: C, 73.4; H, 7.2; N, 19.4.

Synthesis of *N*,*N*-(di-2-pyridyl)-hexylamine (dpha). 2,2′-Dipyridylamine (0.69 g, 4 mmol) was added to a suspension of potassium hydroxide (1.00 g, 18 mmol) in 10 mL of DMSO and stirred at room temperature for 45 min. Afterwards, iodohexane (0.39 mL, 4 mmol) was added to the reaction mixture and stirred at room temperature for 1 h. The reaction was quenched by addition of water (50 mL), and was extracted with diethyl ether for three times (3 × 50 mL). The combined organic extract was dried with magnesium sulfate and filtered. After the removal of solvent of the filtrate under reduced pressure, the crude yellow oily product was obtained and purified by flash column chromatography (SiO_2) with petroleum ether/ethyl acetate (10:1) as eluent. Pale yellow oil was yielded after solvent was removed. Yield: 0.77 g (75%). ^{1}H NMR (400 MHz, $CDCl_3$): δ 0.85 (t, 3H, *J* = 6.9 Hz), 1.32 (m, 6H), 1.68 (m, 2H), 4.16 (t, 2H, *J* = 7.6 Hz), 6.83 (t, 2H, *J* = 5.2 Hz), 7.07 (d, 2H, *J* = 8.3 Hz), 7.50 (t, 2H, *J* = 8.7 Hz), 8.34 (d, 2H, *J* = 4.8 Hz). ^{13}C NMR (100 MHz, $CDCl_3$): δ 14.17, 22.78, 26.87, 28.43, 31.80, 48.55, 114.86, 116.91, 137.17, 148.46, 157.71. ESI-MS: *m/z* 256 $(M+H)^+$.

Synthesis of *N*,*N*-(di-2-pyridyl)-octylamine (dpoa). 2,2′-Dipyridylamine (**dpa**) (0.69 g, 4 mmol) was added to a suspension of potassium hydroxide (1.00 g, 18 mmol) in 10 mL of DMSO

and stirred for 45 min at room temperature. Afterwards, iodooctane (0.72 mL, 4 mmol) was added to the reaction mixture and stirred at room temperature for 12 h. The reaction was quenched by addition of water (50 mL), and was extracted with diethyl ether for three times (3 × 50 mL). The combined organic extract was dried with magnesium sulfate and filtered. After removal of solvent of the filtrate under reduced pressure, the crude yellow oily product was purified by flash column chromatography (SiO_2) with petroleum ether/ethyl acetate (10:1) as eluent. Pale yellow oil was yielded after solvent was removed. Pale yellow oil was yielded after solvent was removed. Yield: 0.80 g (70%). ^{1}H NMR (400 MHz, $CDCl_3$): δ 0.86 (t, 3H, J = 6.6 Hz), 1.29 (m, 10H), 1.68 (m, 2H), 4.15 (d, 1H, J = 7.7 Hz), 4.17 (d, 1H, J = 7.6 Hz), 6.83 (t, 2H, J = 5.1 Hz), 7.07 (d, 2H, J = 8.4 Hz), 7.50 (t, 2H, J = 8.4 Hz), 8.33 (d, 2H, J = 4.7 Hz). ^{13}C NMR (100 MHz, $CDCl_3$): δ 14.17, 22.78, 26.87, 28.43, 31.80, 48.55, 114.86, 116.91, 137.17, 148.46, 157.71. ESI-MS: *m/z* 285 $(M+H)^+$.

General procedures for the synthesis of [Ru(tpy)(L)Cl](CF_3SO_3) (L = κ^2-*N*,*N*-dppa and κ^2-*N*,*N*-dpha). The ethanolic solution (40 mL) of Ru(tpy)Cl_3 (0.33 g, 0.68 mmol), **L** (0.75 mmol) and LiCl (0.5 g, 11.8 mmol) was degassed under N_2, and was refluxed for 1 h under N_2. After the addition of triethylamine (1 mL), the solution was further refluxed for 3 h. The reaction mixture was cooled to room temperature afterwards. Any insoluble solids were removed by filtration and the filtrate was concentrated to ~10 mL under reduced pressure. Addition of saturated aqueous lithium trifluoromethanesulfonate solution to the concentrated solution afforded purple microcrystals. The microcrystals were collected by filtration, washed with cold water and diethyl ether successively and then dried in air.

Complex 1a(CF_3SO_3): [Ru(tpy)(κ^2-*N*,*N*-**dppa**)Cl](CF_3SO_3). Yield: 0.3 g (65%). ^{1}H NMR (400 MHz, $CDCl_3$): δ 0.98 (t, 3H, J = 8.0 Hz), 1.25 (m, 2H), 3.93 (t, 2H, J = 7.7 Hz), 6.67 (d, 1H, J =

4.0 Hz), 6.81 (d, 1H, *J* = 4.0 Hz), 7.07 (d, 1H, *J* = 8.0 Hz), 7.38 (t, 2H, *J* = 4.0 Hz), 7.46 (t, 1H, *J* = 8.0 Hz), 7.54 (t, 1H, *J* = 4.0 Hz), 7.58 (t, 1H, *J* = 8.0 Hz), 7.89 (t, 2H, *J* = 8.0 Hz), 7.98 (t, 1H, *J* = 8.0 Hz), 8.11 (t, 1H, *J* = 8.0 Hz), 8.25 (d, 2H, *J* = 4.0 Hz), 8.32 (m, 2H), 9.76 (d, 1H, *J* = 4.0 Hz). IR (cm^{-1}, KBr pellet): 3447 (w), 3075 (w), 2963 (w), 2932 (w), 2873 (w), 1597 (m), 1570 (w), 1486 (w), 1464 (m), 1443 (m), 1382 (m), 1347 (m), 1284 (s), 1275 (s), 1257 (s), 1225 (m), 1168 (m), 1159 (m), 1138 (m), 1030 (s), 894 (w), 792 (w), 764 (m), 636(m). UV–Vis [λ_{max}, nm (ε, $M^{-1}cm^{-1}$) in CH_3CN]: 239 (25600), 277 (27300), 320 (24100), 368 (br), 502 (br), 543 (br) (4600). ESI-MS: *m/z* 583 $(M-CF_3SO_3^-)^+$. Elemental analysis calc. for $C_{29}H_{26}ClF_3N_6O_3RuS$: C, 47.6; H, 3.6; N, 11.5. Found C, 47.7; H, 3.7; N, 11.4.

Complex 2a(CF_3SO_3): [Ru(tpy)(κ^2-*N*,*N*-**dpha**)Cl](CF_3SO_3). Yield: 0.27 g (70%). ^{1}H NMR (400 MHz, $CDCl_3$): δ 0.88 (t, 3H, *J* = 4.0 Hz), 1.22 (m, 6H), 1.36 (m, 2H), 3.95 (m, 2H), 6.65 (t, 1H, *J* = 4.0 Hz), 6.81 (d, 1H, *J* = 4.0 Hz), 7.05 (d, 1H, *J* = 8.0 Hz), 7.36 (t, 2H, *J* = 4.0 Hz), 7.46 (t, 1H, J = 4.0 Hz), 7.50 (t, 1H, *J* = 8.0 Hz), 7.57 (d, 1H, *J* = 8.0 Hz), 7.89 (t, 2H, *J* = 8.0 Hz), 7.93 (t, 1H, *J* = 8.0 Hz), 8.10 (t, 1H, *J* = 4 Hz), 8.23 (m, 2H), 8.33 (m, 4H), 9.75 (d, 1H, *J* = 4.0 Hz). IR (cm^{-1}, KBr pellet): 3482 (m), 3075 (m), 2927 (m), 2858 (m), 1596 (m), 1571 (w), 1487 (w), 1467 (s), 1446 (s), 1384 (m), 1347 (w), 1273 (s), 1224 (m), 1147 (s), 1031 (s), 922 (w), 771 (s), 674 (w) 636 (s). UV–Vis [λ_{max}, nm (ε, $M^{-1}cm^{-1}$) in CH_3CN]: 240 (23500), 277 (25100), 320 (22100), 368 (br), 502 (br), 546 (br) (4200). ESI-MS: *m/z* 625 $(M-CF_3SO_3)^+$. Elemental analysis calc. for $C_{32}H_{32}ClF_3N_6O_3RuS$: C, 49.6; H, 4.2; N, 10.9. Found: C, 49.1; H, 4.0; N, 10.5.

Synthesis of [Ru(tpy)(dpoa)Cl](ClO4). The ethanolic solution (40 mL) of $Ru(tpy)Cl_3$ (0.33 g, 0.68 mmol), **dpoa** (0.21 g, 0.75 mmol) and LiCl (0.5 g, 11.8 mmol) was degassed under N_2, and was refluxed for 1 h under N_2. After the addition of triethylamine (1 mL), the solution was further refluxed for 3 h. The reaction mixture was cooled to room temperature afterwards. Any

insoluble solids were removed by filtration and the filtrate was concentrated to ~10 mL under reduced pressure. Addition of saturated aqueous lithium perchlorate solution to the concentrated solution afforded purple microcrystals. The microcrystals were collected by filtration, washed with cold water and diethyl ether successively, and dried in air. Yield: 0.43 g (84%).^{1}H NMR (400 MHz, $CDCl_3$): δ 0.86 (t, 2H, *J* = 8.0 Hz), 1.29 (m, 10H), 1.68 (m, 2H), 4.16 (t, 2H, *J* = 8.0 Hz), 6.48 (d, 1H, *J* = 6.4 Hz), 6.89 (d, 1H, *J* =5.6 Hz), 7.13 (d, 1H, *J* = 8.2 Hz), 7.50 (t, 1H, *J* = 7.5 Hz), 7.58 (m, 3H), 8.07 (t, 2H, *J* = 7.6 Hz), 8.16 (t, 1H, *J* = 8.0 Hz), 8.25 (t, 1H, *J* = 7.4 Hz), 8.42 (d, 2H, *J* = 4 Hz), 8.50 (t, 1H, *J* = 8.7 Hz), 8.55 (t, 1H, *J* = 7.9 Hz), 8.58 (d, 2H, *J* = 8.0 Hz), 9.00 (d, 1H, *J* = 5.0 Hz). IR (cm^{-1}, KBr pellet): 3430 (m), 2952 (w), 2927 (w), 2869 (w), 1599 (w), 1559 (w), 1489 (w), 1465 (m), 1447 (m), 1387 (w), 1289 (s), 1238 (s), 1196 (m), 1029 (s), 790 (w), 769 (m), 637 (m). UV–Vis [λ_{max}, nm (ε, $M^{-1}cm^{-1}$) in CH_3CN]: 232 (56446), 273 (73724), 315 (66766), 357 (sh), 488 (br) (11422), 560 (sh). ESI-MS: *m/z* 650 $(M-ClO_4^-)^+$. Elemental analysis calc. for $C_{33}H_{33}N_6O_9RuCl_2$: C, 52.86; H, 4.45; N, 11.21. Found: C, 52.44; H, 4.48; N, 11.06.

General procedures for the synthesis of $[Ru(tpy)(L)(OH_2)](CF_3SO_3)_2$ (L = κ²-*N*,*N*-dppa and κ²-*N*,*N*-dpha). $[Ru(tpy)(\mathbf{L})Cl]CF_3SO_3$ complex (0.2 mmol) was completely dissolved in deionized water (20 mL) by heating the solution to 85 °C. Silver trifluoromethanesulfonate (0.06 g, 0.23 mmol) was added to the solution, and the resulting mixture was heated with stir for 1 h. Silver chloride was filtered off after the solution was cooled to room temperature. Excess amount of zinc powder was added to the filtrate, and the solution was gently heated for 10 min. After zinc dust was removed by filtration, trifluoromethanesulfonic acid (2 mL) was added to the filtrate. The resulting solution was chilled overnight in a refrigerator. Dark violet microcrystals were collected by filtration and dried under vacuum.

Complex 1b$(CF_3SO_3)_2$: [Ru(tpy)(κ^2-*N*,*N*-**dppa**)(OH_2)]$(CF_3SO_3)_2$. Yield: 0.1 g (60%). ^{1}H NMR (400 MHz, D_2O): δ 0.91 (t, 3H, *J* = 7.3 Hz), 1.15 (m, 2H), 4.03 (t, 2H, *J* = 7.7 Hz), 6.48 (d, 1H, *J* = 6.4 Hz), 6.89 (d, 1H, *J* =5.6 Hz), 7.13 (d, 1H, *J* = 8.2 Hz), 7.50 (t, 1H, *J* = 7.5 Hz), 7.58 (m, 3H), 8.07 (t, 2H, *J* = 7.6 Hz), 8.16 (t, 1H, *J* = 8.0 Hz), 8.25 (t, 1H, *J* = 7.4 Hz), 8.42 (d, 2H, *J* = 4 Hz), 8.50 (t, 1H, *J* = 8.7 Hz), 8.55 (t, 1H, *J* = 7.9 Hz), 8.58 (d, 2H, *J* = 8.0 Hz), 9.00 (d, 1H, *J* = 5.0 Hz). ^{13}C NMR (100 MHz, D_2O): δ 159.59, 159.45, 158.50, 153.83, 151.77, 151.42, 150.15, 139.34, 138.00, 137.26, 134.86, 127.11, 123.81, 122.80, 120.86, 119.95, 117.03, 116.42, 52.65, 19.56, 10.50. IR (cm^{-1}, KBr pellet): 3430 (m), 2952 (w), 2927 (w), 2869 (w), 1599 (w), 1559 (w), 1489 (w), 1465 (m), 1447 (m), 1387 (w), 1289 (s), 1238 (s), 1196 (m), 1029 (s), 790 (w), 769 (m), 637 (m). UV–Vis [λ_{max}, nm (ε, $M^{-1}cm^{-1}$) in H_2O]: 232 (56446), 273 (73724), 315 (66766), 357 (sh), 488 (br) (11422), 560 (sh). ESI-MS: *m/z* 273 $(M-H_2O-2CF_3SO_3^-)^{2+}$, 697 $(M-H_2O-CF_3SO_3^-)^+$. Elemental analysis calc. for $C_{30}H_{28}F_6N_6O_7RuS_2$: C, 41.7; H, 3.3; N, 9.7. Found: C, 42.8; H, 3.7; N, 10.4.

Complex 2b$(CF_3SO_3)_2$: [Ru(tpy)(κ^2-*N*,*N*-**dpha**)(OH_2)]$(CF_3SO_3)_2$. Yield: 0.075 g (64%).^{1}H NMR (400 MHz, D_2O): δ 0.78 (t, 3H, *J* = 6.8 Hz), 1.00 (m, 2H), 1.11 (m, 4H), 1.25 (m, 2H), 4.03 (m, 2H), 6.43 (t, 1H, *J* = 6.8 Hz), 6.83 (d, 1H, *J* = 4.7 Hz), 7.06 (d, 1H, *J* = 8.4 Hz), 7.44 (t, 1H, *J* = 7.2 Hz), 7.53 (m, 3H), 7.70 (d, 1H, *J* = 8.4 Hz), 8.02 (t, 2H, *J* = 7.7 Hz), 8.10 (t, 1H, *J* = 8.1 Hz), 8.19 (t, 1H, *J* = 7.2 Hz), 8.36 (d, 2H, *J* = 4Hz), 8.45 (t, 2H, *J* = 9.8 Hz), 8.52 (d, 2H, *J* = 8.0 Hz), 8.93 (d, 1H, *J* = 4.5 Hz). ^{13}C NMR (100 MHz, D_2O): δ 159.77, 159.45, 156.69, 154.96, 151.40, 150.10, 148.60, 138.65, 137.84, 127.17, 123.84, 122.80, 120.01, 117.29, 116.34, 30.66, 25.85, 21.61, 13.17. IR (cm^{-1}, KBr pellet): 3415 (m), 2951 (w), 2977 (w), 2869 (w), 1599 (w), 1466 (s), 1447 (m), 1387 (w), 1289 (s), 1238 (s), 1167 (m), 1029 (s), 790 (w), 769 (m), 637 (m). UV-Vis [λ_{max}, nm (ε, $M^{-1}cm^{-1}$) in H_2O]: 231 (38144), 273 (47912), 315/ (43062), 352 (sh), 493

(br) (8316), 577 (sh). ESI-MS: *m/z* 294 $(M-H_2O-2CF_3SO_3^-)^{2+}$, 739 $(M-H_2O-CF_3SO_3^-)^+$. Elemental analysis calc. for $C_{33}H_{34}F_6N_6O_7RuS_2$: C, 43.8; H, 3.8; N, 9.3. Found: C, 44.0; H, 4.0; N, 9.5.

Synthesis of complex 3$(ClO_4)_2$: [Ru(tpy)(**dpoa**)(OH_2)]$(ClO_4)_2$. The complex of [Ru(tpy)(**dpoa**)Cl](ClO_4) (0.2 mmol) was completely dissolved in deionized water (20 mL) by heating the solution to 85 °C. Silver perchlorate (0.048 g, 0.23 mmol) was added to the solution, and the resulting mixture was heated with stir for 1 h. Silver chloride was filtered off after the solution was cooled to room temperature. Excess amount of zinc powder was added to the filtrate, and the solution was gently heated for 10 min. After zinc dust was removed by filtration, perchloric acid (2 mL) was added to the filtrate. The resulting solution was chilled overnight in a refrigerator. Dark violet microcrystals were collected by filtration and dried under vacuum. Pure Ru-complex **3**$(ClO_4)_2$ was obtained by recrystallization and the crystalline collected was found insoluble in the deuterated solvents. As a result, it was unable to be characterized by NMR. Other characterizations including FTIR, CHN elemental analysis, and *X*-ray crystallography of the complex were acquired successfully. The analytical results were found in good agreement with the proposed structure. Yield: 0.1 g (60%). IR (cm^{-1}, KBr pellet): 3430 (m), 2952 (w), 2927 (w), 2869 (w), 1599 (w), 1559 (w), 1489 (w), 1465 (m), 1447 (m), 1387 (w), 1289 (s), 1238 (s), 1196 (m), 1029 (s), 790 (w), 769 (m), 637 (m). Elemental analysis calc. for $C_{33}H_{35}N_6O_9RuCl_2$: C, 47.53; H, 4.24; N, 10.08. Found: C, 47.64; H, 4.30; N, 10.24.

X-ray crystal structure determination. A single crystal of each complex, **1a**(CF_3SO_3), **1b**$(ClO_4)_2$, **2a**(CF_3SO_3), **2b**$(CF_3SO_3)_2$ and **3**$(ClO_4)_2$, was mounted on a Bruker CCD area detector. With the generator conditions functioning at 50 kV and 30 mA, MoKα radiation (λ = 0.71073 Å) was applied to each sample and the intensity data were collected from 0 to 180

degree. An empirical adsorption was taken in four shells with 1,321 frames. Correction was done by the SADABS (Sheldrick, 1996) program that is based on Fourier coefficient fitting method. The crystal structures were determined by a combination of direct method, which can determine part of non-hydrogen atoms, and Difference Fourier Synthesis method, which can locate all the remaining non-hydrogen atoms. The remaining hydrogen atoms in the crystal structures were located based on Difference Fourier Synthesis while connected with geometrical analysis. All of non-hydrogen atoms were refined anisotropically with weight function,

$$W = \frac{q}{\sigma^2(F_0^2) + (a \times p)^2 + (b \times p) + d + (e \cdot sin\theta)}$$

$$\text{where } p = [f \times \max\ of\ (0\ or\ F_0^2) + (1 - f) \times F_c^2]$$

The position of hydrogen atoms was refined with fixed individual displacement parameters. All experiments and computations were performed on a Bruker CCD Area Detector Diffractometer and a computer with the Bruker Smart software and Bruker Shelxtl program packages. The crystallographic data as well as detailed refinement procedures are reported in Table S1 in the supporting information. Data of the complexes were deposited to CCDC with CCDC number 1546191–1546195. These data can be obtained free of charge from The Cambridge Crystallographic Data Center via www. Ccdc.cam.uk/data_request/cif.

RESULTS AND DISCUSSION

Synthesis and spectroscopic characterizations of the Ru-complexes. The *N*-substituted 2,2′-dipyridylamine ligands and their corresponding Ru^{II} aqua complexes $[Ru(tpy)(\mathbf{L})(OH_2)]^{2+}$ were prepared by multi-step synthesis as outlined in Scheme 1.[60, 61, 62] The ligands **dppa** and **dpha** were obtained in moderate yields from the reaction of 2,2′-dipyridylamine and alkyl iodide in the presence of potassium hydroxide as a base at room temperature. Further reaction of the ligand (**L**) with terpyridine-ruthenium trichloride[59] ($[Ru(tpy)Cl_3]$) afforded an intermediate $[Ru(tpy)(\mathbf{L})Cl]Cl$. The new Ru^{II}-aqua complexes $[Ru(tpy)(\mathbf{L})(OH_2)](CF_3SO_3)_2$ were then obtained by removing the chloro ligand from $[Ru(tpy)(\mathbf{L})Cl]Cl$ with silver trifluoromethanesulfonate in aqueous solution. Zinc dust was used to remove the excess silver ions in the reaction. The Ru^{II}-aqua complexes were further purified by re-crystallization to afford dark purple microcrystals and then were characterized by IR, ESI-MS, ^1H NMR and elemental analysis.

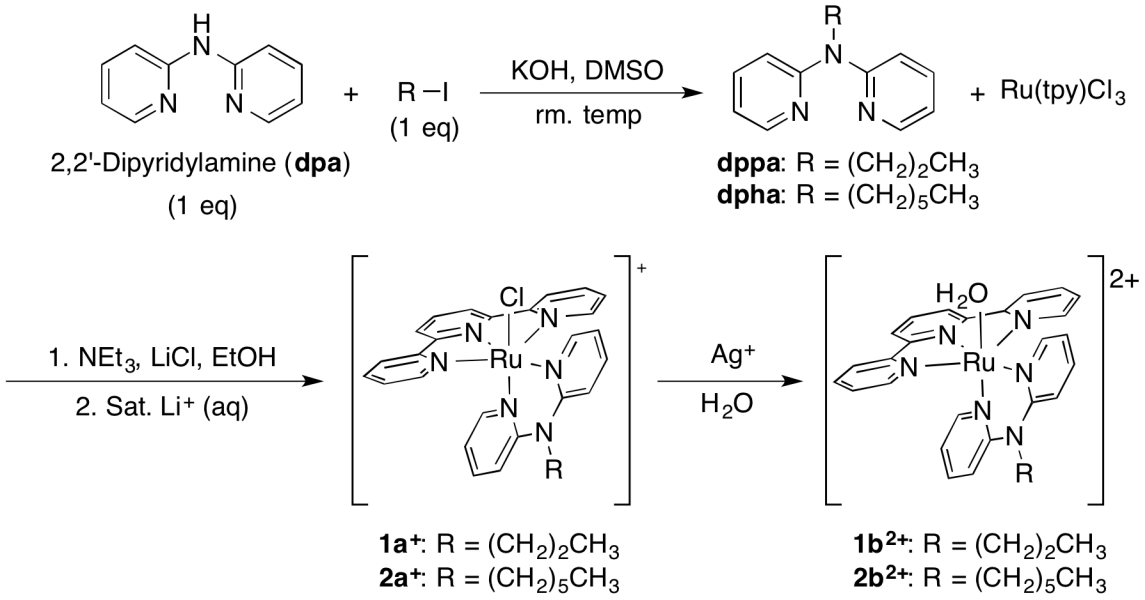

Scheme 1. Synthetic routes to *N*-substituted 2,2′-dipyridylamine ligands (**dppa** and **dpha**) and Ru^{II}-aqua complex.

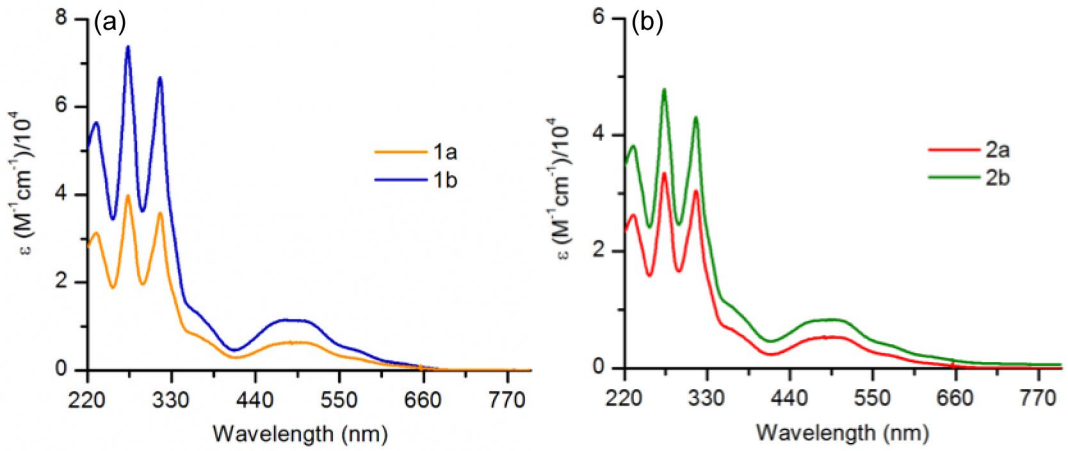

Figure 1. UV-Vis absorption spectra of Ru^{II}-chloro complexes and their corresponding Ru^{II}-aqua complexes in water: (a) [**1a**]$^{+}CF_3SO_3^{-}$ and [**1b**]$^{2+}(CF_3SO_3^{-})_2$; (b) [**2a**]$^{+}CF_3SO_3^{-}$ and [**2b**]$^{2+}(CF_3SO_3^{-})_2$.

The UV-Vis absorption spectra of [Ru(tpy)(**L**)(Cl)]CF_3SO_3 and [Ru(tpy)(**L**)(OH_2)]$(CF_3SO_3)_2$ complexes were shown in Figure 1. Comparing with **L**, both complexes [**1b**]$^{2+}(CF_3SO_3^{-})_2$ and [**2b**]$^{2+}(CF_3SO_3^{-})_2$ show the new and broad absorption peaks in the range of 482–600 nm, which are assigned to metal-to-ligand charge transfer (MLCT). The intense absorption peaks observed in the range of 230–360 nm are assigned to intra-ligand π–π* transitions. It is noteworthy that the MLCT absorption bands of the Ru^{II}-aqua complexes in the visible region do not shift compared to their corresponding Ru^{II}-chloro complexes ([**1a**]$^{+}CF_3SO_3^{-}$ and [**2a**]$^{+}CF_3SO_3^{-}$). This observation is interestingly different from a similar Ru^{II}-complex system reported in literature[63] and their MLCT absorption bands of [Ru(tpy)(**dpa**)X]$^{n+}$ (X = Cl^{-}, H_2O; n = 1, 2) complexes are blue-shifted (about 34 nm) upon the replacement of the coordinated chloro ligand by a water molecule. This indicates that the MLCT band energy of the Ru^{II}-aqua complex is increased. However, our Ru^{II}-aqua complexes coordinated with the ligands **dppa** or **dpha** possessing an alkyl chain substituted on the 2,2′-dipyridylamine (**dpa**) moiety show no changes in MLCT band

energy, which indicate that the alkyl chain tagged in the ligand may contribute an significant electron-donating strength to the Ru^{II}-aqua complex.

X-ray crystallographic studies of Ru^{II} complexes. Crystallization of an aqueous solution of [**1a**]$^{+}CF_3SO_3^{-}$, [**2a**]$^{+}CF_3SO_3^{-}$, [**1b**]$^{2+}(ClO_4^{-})_2$, [**2b**]$^{2+}(CF_3SO_3^{-})_2$ and [**3b**]$^{2+}(ClO_4^{-})_2$ in the presence of either CF_3SO_3H or $HClO_4$ successfully afforded single crystals that were suitable for X-ray crystallographic studies. The collection and refinement data and the selected bond lengths are shown in Table 1 and the bond angles of the structures are summarized in Table S3 in the supporting information. The structures of the four complexes are similar and display a distorted octahedral geometry. The six-coordinated Ru^{II} metal center is bonded with three nitrogen atoms of terpyridine in meridional position, one chloride ion or one oxygen atom of water molecule at axial position, and two pyridine nitrogen atoms of **dppa** or **dpha**. The alkyl chain is located far from the metal center.

Table 1. Selected bond lengths (Å) of Ru^{II}-complexes.

Bond length	[**1a**]$^{+}(CF_3SO_3^{-})$	[**2a**]$^{+}(CF_3SO_3^{-})$	[**1b**]$^{2+}(ClO_4^{-})_2$	[**2b**]$^{2+}(CF_3SO_3^{-})_2$	[**3**]$^{2+}(ClO_4^{-})_2$
Ru–N1	2.064(3)	2.066(2)	2.0833(13)	2.073(2)	2.076(2)
Ru–N2	1.951(3)	1.9517(19)	1.9569(12)	1.957(3)	1.953(2)
Ru–N3	2.083(3)	2.080(2)	2.0872(13)	2.063(2)	2.067(2)
Ru–N4	2.122(3)	2.118(2)	2.0891(12)	2.102(3)	2.089(2)
Ru–N5	2.077(3)	2.090(2)	2.0445(12)	2.043(3)	2.045(2)
Ru–Cl1	2.3995(11)	2.4009(8)	-	-	-
Ru–O1W	-	-	2.1320(11)	2.136(3)	2.1381(19)

From the Ru^{II}-chloro complexes [**1a**]$^{+}CF_3SO_3^{-}$ and [**2a**]$^{+}(CF_3SO_3^{-})_2$ shown in Figure 2a and b, the Ru–N_{tpy} bond lengths at terpyridine are in the range of 1.951–2.082 Å, which are comparable to that of reported [Ru(tpy)(**dpa**)Cl]$^{+}$ structure.[63] The bite angle of terpyridine in

both [**1a**]$^{+}$ and [**2a**]$^{+}$ is approximately 79°, which is typically found for terpyridine complexes.[63-69] In both structures, the bite angle between the *N*-substituted 2,2′-dipyridylamine ligand and Ru^{II} ion is larger than 80°. The Ru–N_{dppa} bond lengths in [**1a**]$^{+}$ are 2.078 and 2.122 Å while the Ru–N_{dpha} bond lengths in [**2a**]$^{+}$ are 2.090 and 2.118 Å, which are comparable to those of [Ru(tpy)(**dpa**)Cl]$^{+}$ complex. In addition, the Ru–Cl bond lengths in both [**1a**]$^{+}$ and [**2a**]$^{+}$ complexes are 2.40 Å, which is also close to the that of [Ru(tpy)(**dpa**)Cl]$^{+}$. From the crystal structures of Ru^{II}-aqua complexes shown in Figure 3a and b, both [**1b**]$^{2+}$ and [**2b**]$^{2+}$ have very similar Ru–N_{tpy} bond lengths at terpyridine ligand in the range of 1.957–2.087 Å. However, the bond distances in both structures are found slightly shorter than that found in [Ru(tpy)(**dpa**)(OH_2)]$^{2+}$. Moreover, the bite angles of terpyridine in [**1b**]$^{2+}$ and [**2b**]$^{2+}$ were maintained at 79° approximately and are consistent with [Ru(tpy)(**dpa**)(OH_2)]$^{2+}$ and other Ru–tpy complexes.[63-69] The Ru–N_{dppa} bond lengths in complex [**1b**]$^{2+}$ are 2.044 and 2.089 Å, which are also very close to those found in [**2b**]$^{2+}$ (2.043 and 2.102 Å) and [Ru(tpy)(**dpa**)(OH_2)]$^{2+}$. The Ru–O bond length observed form complex [**1b**]$^{2+}$ and [**2b**]$^{2+}$ is 2.13 Å approximately, which is comparable to the Ru^{II}-aqua complex with **dpa** as the ligand (2.126 Å). These results indicate that the alkyl chain tagged in the **dpa** ligand moiety show no significant influence to the coordination property including the bond lengths and bond angles and the geometry of the molecular structure of Ru^{II}–Cl and Ru^{II}–OH_2 complexes.

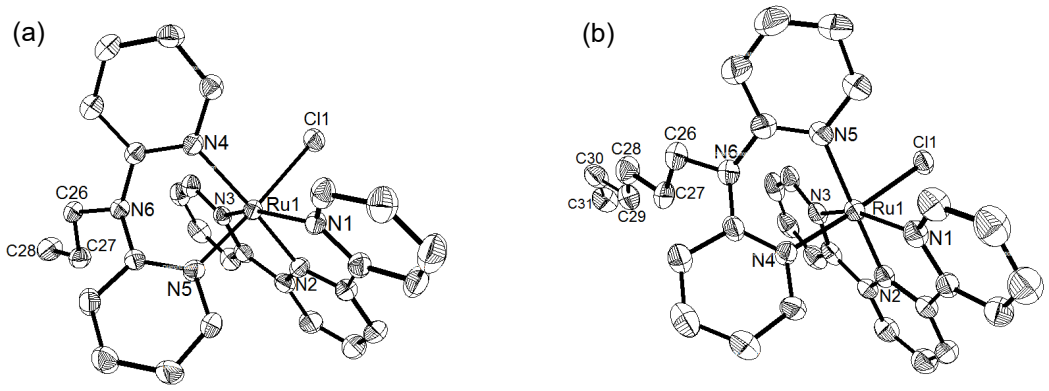

Figure 2. ORTEP view of the Ru^{II}–Cl complexes: (a) [**1a**]$^{+}CF_3SO_3^{-}$ and (b) [**2a**]$^{+}CF_3SO_3^{-}$ (Ellipsoids are drawn at 30% probability) with partial atom labellings. Hydrogen atoms and counterions are omitted for clarity.

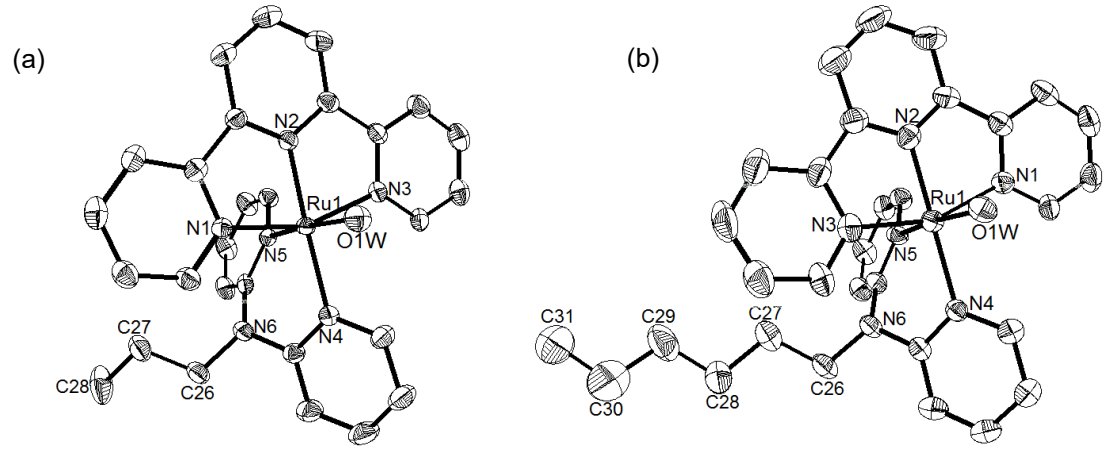

Figure 3. ORTEP view of the Ru^{II}–OH_2 complexes: (a) [**1b**]$^{2+}(ClO_4^{-})_2$ and (b) [**2b**]$^{2+}(CF_3SO_3^{-})_2$ (Ellipsoids are drawn at 30% probability) with partial atom labelling. Hydrogen atoms and counterions are omitted for clarity.

Electrochemical studies of [Ru(tpy)(L)(OH$_2$)]$^{2+}$ complexes. The redox properties of the complexes [Ru(tpy)(**dppa**)(OH$_2$)]$^{2+}$ and [Ru(tpy)(**dpha**)(OH$_2$)]$^{2+}$ in 0.01 M CF_3SO_3H and 0.01 M $HClO_4$ aqueous solution (pH = 2, I = 0.1 M) were analyzed by cyclic voltammetry (CV). The analysis was carried out using a disk GCE as the working electrode. A platinum wire and a

saturated calomel electrode (SCE) were engaged as the counter and the reference electrodes. To emphasize the influence of the alkyl chain tagged in the **dpa** ligand on the electrochemical properties of the Ru^{II}-aqua complex, $[Ru(tpy)(\mathbf{dpa})(OH_2)]^{2+}$ in the same electrolytes was also studied for comparison. The electrochemical properties were summarized in Table 2. The stacked CVs of $[Ru(tpy)(\mathbf{dpa})(OH_2)]^{2+}$, $[\mathbf{1b}]^{2+}$, and $[\mathbf{2b}]^{2+}$ in CF_3SO_3H solution were shown Figure 5a and each complex exhibits one reversible $Ru^{II/III}$ couple at the $E_{1/2}$ (ΔE_p) values of 0.67 V (60), 0.72 V (70), and 0.72 V (70) *vs*. SCE respectively (Table 2). For the analysis carried out in $HClO_4$ solution (Figure 5b), the CVs results were obtained almost same as in CF_3SO_3H solution. The $E_{1/2}$ values obtained were 0.67 V (60) for $[Ru(tpy)(\mathbf{dpa})(OH_2)]^{2+}$, 0.71 V (70) for $[\mathbf{1b}]^{2+}$, and 0.71 V (70) for $[\mathbf{2b}]^{2+}$, indicating that the electrolyte has no influence on the $Ru^{II/III}$ couples. However, it is interesting to find that the redox potential of $Ru^{II/III}$ couple is obviously increased for the Ru^{II}-aqua complexes coordinated with an alkyl-chain tagged ligand (**dppa** in $[\mathbf{1b}]^{2+}$ and **dpha** in $[\mathbf{2b}]^{2+}$), implying that the ligand tagged alkyl-chain can offer better stabilization for $Ru^{II/III}$ complex.

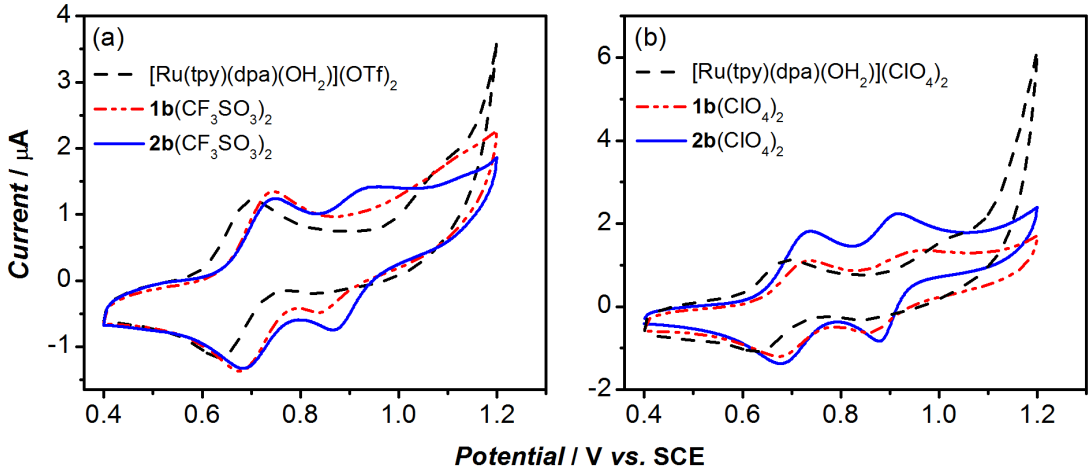

Figure 5. Cyclic voltammograms of $[\mathbf{1b}]^{2+}$, $[\mathbf{2b}]^{2+}$, and $[Ru(tpy)(\mathbf{dpa})(OH_2)]^{2+}$ in (a) 0.01 M CF_3SO_3H and (b) 0.01 M $HClO_4$ aqueous solution (pH = 2, I = 0.1 M) at a scan rate of 20 mVs^{-1}

using a glassy carbon disk as working electrode, a Pt wire as counter electrode, and saturated calomel electrode (SCE) as reference electrode.

More importantly, the CV experiments using $[\mathbf{2b}]^{2+}$ in CF_3SO_3H showed a quasi-reversible wave corresponding to the redox couple of Ru^{III}–OH and Ru^{IV}=O couple at the $E_{1/2}$ value (ΔE_p) of 0.91 V (70) (Table 2) while it is not occurred in the both $[Ru(tpy)(\mathbf{dpa})(OH_2)]^{2+}$ and $[\mathbf{1b}]^{2+}$ complexes (Figure 5a). This is probably because of $[\mathbf{2b}]^{2+}$ complex is coordinated with the ligand tagged with a hexyl chain, which facilitates the electrochemical interconversion between Ru^{III}–OH and Ru^{IV}=O redox couples, meaning that the Ru^{IV}=O formation from $[\mathbf{2b}]^{2+}$ is more favorable than $[Ru(tpy)(\mathbf{dpa})(OH_2)]^{2+}$. When the CV experiments were performed in $HClO_4$ solution (Figure 5b), $[Ru(tpy)(\mathbf{dpa})(OH_2)]^{2+}$ gave no observable $Ru^{III/IV}$ couple, but both $[\mathbf{1b}]^{2+}$ and $[\mathbf{2b}]^{2+}$ produced a remarkable quasi-reversible wave corresponding to $Ru^{III/IV}$ couple at the $E_{1/2}$ (ΔE_p) about 0.90 V (100). The redox couple of $[\mathbf{2b}]^{2+}$ showed an even more intense and sharper current peak with a better-defined couple at $E_{1/2}$ = 0.90 V (Figure 5b, blue line) in $HClO_4$ solution than in CF_3SO_3H solution. In addition, it is noteworthy that the current peak height of the $Ru^{III/IV}$ couple of $[\mathbf{2b}]^{2+}$ in $HClO_4$ solution is comparable to its $Ru^{II/III}$ couple, which is rarely observed in the polypyridyl Ru^{II}-aqua systems reported in literature.[70-75] This may indicate that the Ru^{II}-aqua complex coordinated with *N*-alkyl substituted dipyridylamine ligand and complementary with a suitable anions could promote the $Ru^{III/IV}$ couple, which is probably due to synergetic effects to stabilize the high valence intermediates and to enhance the electrode surface interactions of complexes in the acidic aqueous media.

Table 2. Redox potentials of Ru^{II}-aqua complexes in 0.01 M CF_3SO_3H and 0.01 M $HClO_4$ solution.

Complex	$CF_3SO_3H_{(aq)}$		$HClO_{4(aq)}$	
	$E_{1/2}$ (V)[a,b] of $Ru^{III/II}$	$E_{1/2}$ (V)[a,b] of $Ru^{IV/III}$	$E_{1/2}$ (V)[a,b] of $Ru^{III/II}$	$E_{1/2}$ (V)[a,b] of $Ru^{IV/III}$
$[Ru(tpy)(\mathbf{dpa})(OH_2)]^{2+}$	0.67	-	0.67	-
$[\mathbf{1b}]^{2+}$	0.72	-	0.71	0.91[c]
$[\mathbf{2b}]^{2+}$	0.72	0.91[c]	0.71	0.90[c]

[a] Measured by cyclic voltammetry, $E_{1/2} = (E_{pa} + E_{pc})/2$.
[b] The potential reported were reference to SCE.
[c] Quasi-reversible couple.

To investigate further the perchlorate effect on promoting the $Ru^{III/IV}$ couple, CVs of $[\mathbf{1b}]^{2+}$ in 0.01 M CF_3SO_3H solution with the increasing concentration of perchlorate anion were conducted. As shown in Figure 6, $[\mathbf{1b}]^{2+}$ only showed a weak and irreversible reduction peak potential at 0.84 V in CF_3SO_3H solution, while adding perchlorate ions (0.07 M), the $Ru^{III/IV}$ couple appeared obviously. As increasing concentration up to 0.21 M, the peak size of the $Ru^{III/IV}$ couple reached its maximum and further addition leads to $[\mathbf{1b}]^{2+}$ precipitation. We further extended the potential scanning range to 1.8 V to examine whether the formation of Ru^{V} species could be promoted under these conditions. However, no noticeable $Ru^{IV/V}$ couple was observed (cyclic voltammogram shown in Figure S6). From these CV experiments, the presence of perchlorate anion evidently promotes $Ru^{III/IV}$ couple as indicated by the distinctive peak size and shape of the couple from the cyclic voltammogram. The mechanism behind the enhancement of $Ru^{III/IV}$ couple with perchlorate anion is not clear. However, we speculate that it could be related to the stability of the *in-situ* generated high-valent Ru^{IV}=O species. During the redox reaction, polar solvent molecules (H_2O) that are surrounding the unstable Ru^{IV}=O intermediate will compete with the anions of the complexes for coordination. The successful coordinated H_2O

molecule donates lone-pair electrons from the oxygen atom to stabilize the highly electron-deficient Ru^{IV}=O species.[76] Since the triflate anion may compete with H_2O molecule to form an inner-sphere complex with cationic high-valent Ru-oxo species, the formation of Ru^{IV}=O species is thus hindered.[77] On the contrary, apart from the outer-sphere intrinsic cation–anion interaction, perchlorate anion is always dissociated from metal complex.[77] Therefore, it does not compete with H_2O molecule to form inner-sphere complex with the high-valent Ru center during the redox process of $Ru^{III/IV}$ couple. Consequently, the promotion of redox $Ru^{III/IV}$ couple is more feasible and observable in perchlorate solution than that of triflate as shown in Figure 5b and Figure 6.

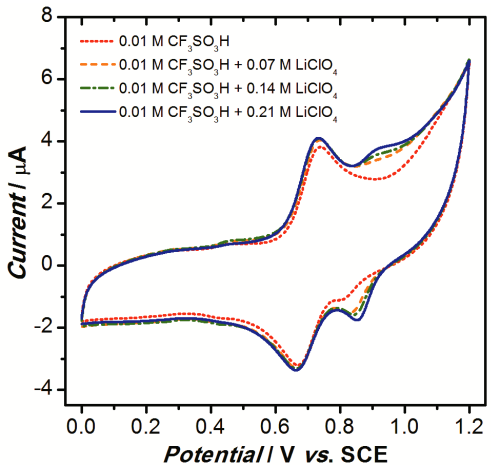

Figure 6. Stacked CVs of $[\mathbf{1b}]^{2+}$ measured in 0.01 M CF_3SO_3H aqueous solution (pH = 2, I = 0.1 M) in the presences of different amount of $LiClO_4$ at a scan rate of 100 mVs^{-1}.

To obtain the thermodynamic information on the proton-coupled electron transfers of the new Ru^{II}-aqua complexes, the Pourbaix diagrams were constructed and shown in Figure 7. The CV experiments were carried out with $[\mathbf{1b}]^{2+}$ and $[\mathbf{2b}]^{2+}$ and the $E_{1/2}$ versus SCE was measured as a function of pH in the range of 0 to 14 with addition of perchlorate anions. Similar to other reported ruthenium-aqua complexes, the $E_{1/2}$ of $Ru^{II/III}$ couples of $[\mathbf{1b}]^{2+}$ and $[\mathbf{2b}]^{2+}$ are 0.72 and

0.76 V respectively, which are independent of pH under strong acidic conditions (pH < 2.0).[72, 74, 78, 79] Moreover, the $E_{1/2}$ of $Ru^{III/IV}$ couple of $[\mathbf{1b}]^{2+}$ and $[\mathbf{2b}]^{2+}$ decreases by 124 mV per pH unit, indicating that it is an one-proton, two-electrons process.

pH < 2.0

$[Ru^{III}(tpy)(\kappa^2\text{-}N,N\text{-dppa})(OH_2)]^{3+} + e^- \rightleftharpoons [Ru^{II}(tpy)(\kappa^2\text{-}N,N\text{-dppa})(OH_2)]^{2+}$

$[Ru^{IV}(tpy)(\kappa^2\text{-}N,N\text{-dppa})O]^{2+} + e^- + 2H^+ \rightleftharpoons [Ru^{III}(tpy)(\kappa^2\text{-}N,N\text{-dppa})(OH_2)]^{3+}$

$[Ru^{III}(tpy)(\kappa^2\text{-}N,N\text{-dpha})(OH_2)]^{3+} + e^- \rightleftharpoons [Ru^{II}(tpy)(\kappa^2\text{-}N,N\text{-dpha})(OH_2)]^{2+}$

$[Ru^{IV}(tpy)(\kappa^2\text{-}N,N\text{-dpha})O]^{2+} + e^- + 2H^+ \rightleftharpoons [Ru^{III}(tpy)(\kappa^2\text{-}N,N\text{-dpha})(OH_2)]^{3+}$

From pH 2 to 10, the $E_{1/2}$ of $Ru^{II/III}$ and $Ru^{III/IV}$ couples of $[\mathbf{1b}]^{2+}$ and $[\mathbf{2b}]^{2+}$ decreases by 59 mV per pH unit, an indicative of one-proton, one-electron process.

2.0 < pH <10

$[Ru^{III}(tpy)(\kappa^2\text{-}N,N\text{-}\mathbf{dppa})(OH)]^{3+} + e^- + H^+ \rightleftharpoons [Ru^{II}(tpy)(\kappa^2\text{-}N,N\text{-}\mathbf{dppa})(OH_2)]^{2+}$

$[Ru^{IV}(tpy)(\kappa^2\text{-}N,N\text{-}\mathbf{dppa})O]^{2+} + e^- + H^+ \rightleftharpoons [Ru^{III}(tpy)(\kappa^2\text{-}N,N\text{-}\mathbf{dppa})(OH)]^{2+}$

$[Ru^{III}(tpy)(\kappa^2\text{-}N,N\text{-}\mathbf{dpha})(OH)]^{2+} + e^- + H^+ \rightleftharpoons [Ru^{II}(tpy)(\kappa^2\text{-}N,N\text{-}\mathbf{dpha})(OH_2)]^{2+}$

$[Ru^{IV}(tpy)(\kappa^2\text{-}N,N\text{-}\mathbf{dpha})O]^{2+} + e^- + H^+ \rightleftharpoons [Ru^{III}(tpy)(\kappa^2\text{-}N,N\text{-}\mathbf{dpha})(OH)]^{2+}$

At pH > 10, the slope for $Ru^{III/IV}$ couple in the Poubaix diagram remains at 60 mV/pH. For $Ru^{II/III}$ couple, it becomes zero and is independent of pH.

pH > 10

$[Ru^{III}(tpy)(\kappa^2\text{-}N,N\text{-}\mathbf{dppa})(OH)]^{2+} + e^- \rightleftharpoons [Ru^{II}(tpy)(\kappa^2\text{-}N,N\text{-}\mathbf{dppa})(OH)]^{2+}$

$[Ru^{IV}(tpy)(\kappa^2\text{-}N,N\text{-}\mathbf{dppa})O]^{2+} + e^- + 2H^+ \rightleftharpoons [Ru^{III}(tpy)(\kappa^2\text{-}N,N\text{-}\mathbf{dppa})(OH_2)]^{2+}$

$[Ru^{III}(tpy)(\kappa^2\text{-}N,N\text{-}\mathbf{dpha})(OH)]^{2+} + e^- \rightleftharpoons [Ru^{II}(tpy)(\kappa^2\text{-}N,N\text{-}\mathbf{dpha})(OH)]^{2+}$

$[Ru^{IV}(tpy)(\kappa^2\text{-}N,N\text{-}\mathbf{dpha})O]^{2+} + e^- + 2H^+ \rightleftharpoons [Ru^{III}(tpy)(\kappa^2\text{-}N,N\text{-}\mathbf{dpha})(OH_2)]^{2+}$

Based on the Pourbaix diagrams, the estimated pK_a values for [**1b**]$^{3+}$ and [**1b**]$^{2+}$ are 1.9 and 9.9, respectively. Similar pK_a values are also obtained with [**2b**]$^{3+}$ and [**2b**]$^{2+}$. Therefore, the length of the alkyl chain substituted on the ligand shows no influence to the pK_a values. In addition, the pK_a values of the new Ru-complexes are found very comparable to those reported Ru-complexes based on poly-pyridyl ligand system including [Ru^{III}(tpy)(bpy)(OH_2)]$^{3+}$ and [Ru^{II}(tpy)(bpy)(OH_2)]$^{2+}$ (pK_a = 1.7 and 9.7, respectively),[78] [Ru^{III}(bpea)(bpy)(OH_2)]$^{3+}$ and [Ru^{II}(bpea)(bpy)(OH_2)]$^{2+}$ (bpea = *N*,*N*-bis(2-pyridylmethyl)ethylamine, pK_a = 1.2 and 11.1, respectively),[42] and [Ru^{III}(tpy)(κ^2-*N*,*N*-PPP)(OH_2)]$^{3+}$ and [Ru^{II}(tpy)(κ^2-*N*,*N*-PPP)(OH_2)]$^{2+}$ (PPP = *N*-(3-*N*,*N*′-bis(2-pyridyl)aminopropyl)pyrrole, pK_a = 1.7 and 10, respectively).[62]

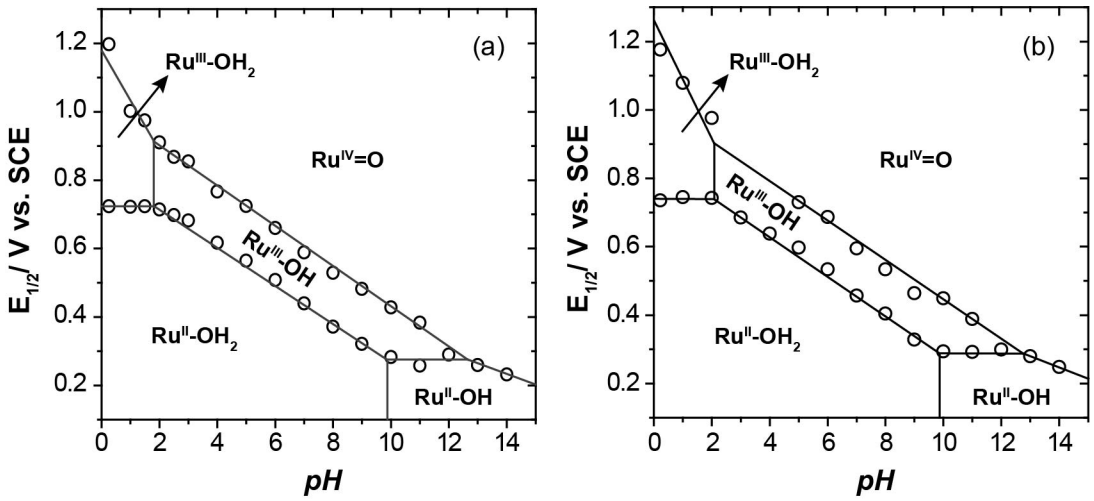

Figure 7. Pourbaix diagram for the Ru^{II}-aqua complexes of (a) [**1b**]$^{2+}$ and (b) [**2b**]$^{2+}$ showing the pH dependence of $E_{1/2}$ versus SCE. The vertical lines indicate the estimated pK_a values for lower oxidation state.

The enhancement of Ru^{III}–OH_2 to Ru^{IV}=O couple formation may be also attributed from the improved adsorption ability of the Ru complexes coordinated with the ligand bearing an alkyl chain such as *n*-propyl, *n*-hexyl and *n*-octyl. With respect to the CV experiments shown in Figure 5, it indicated that the hexyl chain ([**2b**]$^{2+}$) promotes the redox $Ru^{III/IV}$ couple better than that of

propyl chain ([**1b**]$^{2+}$), whereas the redox couple cannot be observed from the complex ([Ru(tpy)(**dpa**)(OH_2)]$^{2+}$) without an alkyl chain on the **dpa** ligand. A longer carbon chain may be able to improve the surface adsorption ability further. We thus prepared a Ru^{II}-aqua complex [**3**]$^{2+}$ coordinated with 2,2′-dipyridyl-*n*-octylamine ligand (**dpoa**, with an octyl chain). The X-ray crystal structure of the complex ([Ru(tpy)(κ^2-N,N-**dpoa**)(OH_2)]$^{2+}$) was obtained and was shown in Figure 8. The CVs of [**3**]$^{2+}$ measured in 0.01 M $HClO_4$ (aq) also showed two quasi-reversible waves (Figure 9a) similar to [**1b**]$^{2+}$ and [**2b**]$^{2+}$. The couple of $E_{1/2}$ (ΔE_p) at 0.73 V (50) is assigned to $Ru^{II/III}$ couple and the other one with $E_{1/2}$ (ΔE_p) at 0.86 V (60) is assigned to $Ru^{III/IV}$ couple. These couples are found slightly shifted to cathodic compared to [**1b**]$^{2+}$ and [**2b**]$^{2+}$ under the same conditions. In addition, a sharper reduction wave of $Ru^{III/IV}$ couple is observed in [**3**]$^{2+}$ (Figure 9a). The reduction wave indicates evidently the occurrence of complex adsorption onto the surface of electrode.[80] This observation is further supported by the repetitive CV measurements of transferred electrode in a clean electrolyte of 0.01 M $HClO_4$. As shown in Figure 8b, at the first scan, the $Ru^{II/III}$ and $Ru^{III/IV}$ couples are clearly observed, which indicate the adsorption of the Ru-complex onto the electrode surface. However, the redox couples diminish progressively during the five continuous cycles, indicating that the high-valent complex is not robust. This may imply that the increasing the carbon chain length of the alkyl group could improve the surface adsorption ability but at same time reducing the stability of the Ru-complex in high oxidation state.

In addition, the double-step chronocoulometry of Ru(tpy)(**dpa**)(OH_2)]$^{2+}$, [**1b**]$^{2+}$ and [**2b**]$^{2+}$ was also performed in 0.01 M CF_3SO_3H (pH = 2, I = 0.1 M) solution in the absence and presence of perchlorate anion. The charge of absorbed species (Q_{ads}) and the calculated amount of absorbed species (Γ_R) on the GCE surface based on Anson plots were summarized in Table 3.

Under the conditions without using perchlorate, the amount of absorbed species on the electrode surface increases with respect to the length of the alkyl chain substituted to **dpa** ligand (*i.e.* **dpha** > **dppa** > **dpa**). A similar trend is also observed in the presence of 0.14 M perchlorate anion. It is noteworthy that all these complexes show significant increase for the amounts of absorbed Ru-species onto the electrode surface under the conditions with perchlorate anion.

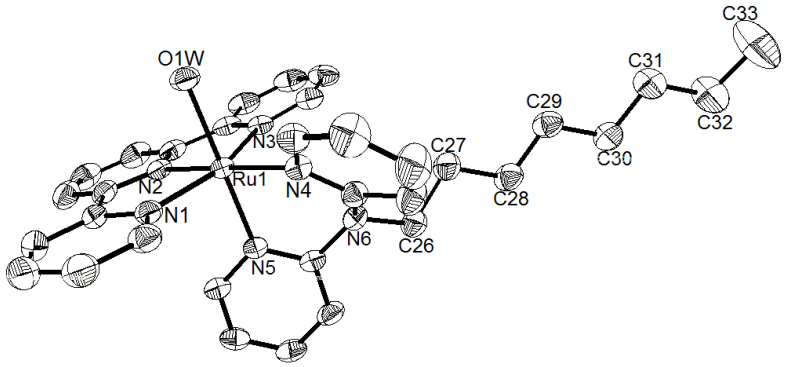

Figure 8. ORTEP view of $[\mathbf{3}]^{2+}(ClO_4^-)_2$ (Ellipsoids are drawn at 30% probability) with partial atom labelling. Hydrogen atoms and counterions are omitted for clarity.

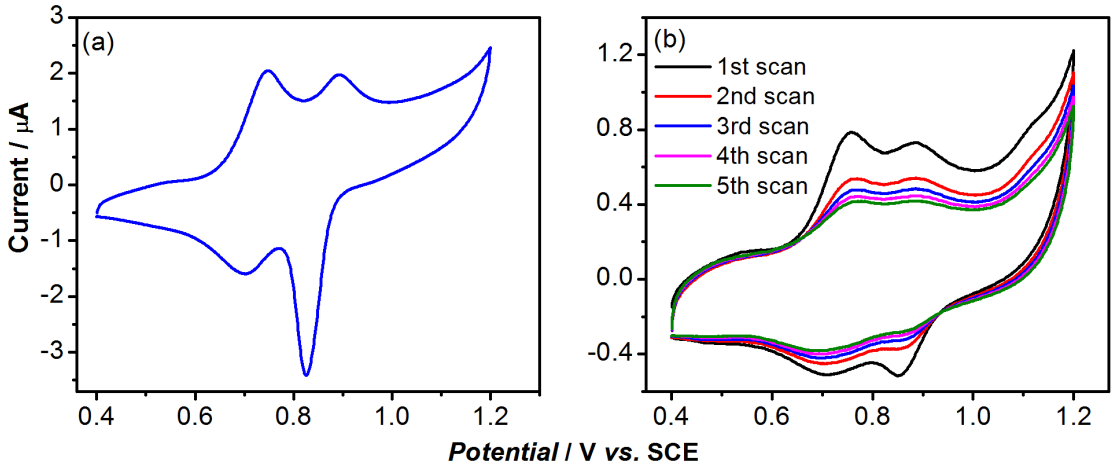

Figure 9. (a) Cyclic voltammogram of $[\mathbf{3}]^{2+}$ in 0.01 M $HClO_4$ aqueous solution (pH = 2, I = 0.1 M) at a scan rate of 20 mVs^{-1} using a glassy carbon disk as working electrode. (b) Repetitive

cyclic voltammetric scans using the GC disk working electrode with absorbed $[\mathbf{3}]^{2+}$ in neat 0.01 M $HClO_4$ aqueous solution.

Table 3. Summary of the charge of absorbed species (Q_{ads}) and the amount of absorbed Ru^{II}-aqua complexes (Γ_R) $[Ru(tpy)(\mathbf{dpa})(OH_2)]^{2+}$, $[\mathbf{1b}]^{2+}$ and $[\mathbf{2b}]^{2+}$ on the disk GCE (surface area = 0.07 cm^2). Data were obtained from Anson plots based on double-step chronocoulometry.

Complex	No $LiClO_4$		With 0.14 M $LiClO_4$	
	Q_{ads} (μC)[a]	$\Gamma_R \times 10^6$ (μmol cm^{-2})[b]	Q_{ads} (μC)[a]	$\Gamma_R \times 10^6$ (μmol cm^{-2})[b]
$[Ru(tpy)(\mathbf{dpa})(OH_2)]^{2+}$	0.079 (± 0.020)	11.72 (± 3.02)	0.200 (± 0.046)	29.54 (± 6.88)
$[\mathbf{1b}]^{2+}$	0.088 (± 0.028)	13.10 (± 4.09)	0.227 (± 0.045)	33.67 (± 6.61)
$[\mathbf{2b}]^{2+}$	0.093 (± 0.027)	13.73 (± 4.04)	0.249 (± 0.17)	36.90 (± 25.79)
Blank	-	-	-	-

[a] Calculated by subtracting *y*-intercept value of the reverse step from the forward step in chronocoulometric plots. [b] $\Gamma_R = Q_{ads}/nFA$.

Table 4. Results of electrocatalytic water oxidation using Ru^{II}-aqua complex as the catalyst.

Complex	Charge (C)	Amount of O_2 generated (μmol)
$[Ru(tpy)(\mathbf{dpa})(OH_2)](ClO_4)_2$	30.31	2.7
$\mathbf{1b}(ClO_4)_2$	33.20	4.1
$\mathbf{2b}(ClO_4)_2$	34.25	0.9

Investigation of the Ru^{II}-aqua complexes in electrocatalytic water oxidation. The bulk electrolysis was with 0.075 mM Ru^{II}-aqua complex ($[Ru(tpy)(\mathbf{dpa})(OH_2)](ClO_4)_2$, $\mathbf{1b}(ClO_4)_2$, or $\mathbf{2b}(ClO_4)_2$) as the catalyst at 2.0 V conducted in a pH 5.0 aqueous solution. The results of electrocatalytic water oxidation were summarized in Table 4. In general, the charge density (coulomb, C) obtained from the Ru^{II}–aqua complexes (30 – 34.3 C) show significantly higher than that of the bare electrode (19.12 C). The bulk electrolysis of a blank buffer solution for 2 h only produces 0.1 μmol of dioxygen (O_2), while applying $[Ru(tpy)(\mathbf{dpa})(OH_2)](ClO_4)_2$ as the catalyst, 2.7 μmol of O_2 was produced. When using $\mathbf{1b}(ClO_4)_2$ complex in the electrolysis, 4.1 μmol of O_2 was generated, which is the best catalytic results among the three Ru^{II}-aqua complex

tested under the same conditions. The significant dropped in the electrocatalytic ability for **2b**$(ClO_4)_2$ (0.9 μmol O_2 generated) is possibly due to the non-polar hexyl chain of the ligand reducing the efficiency of electron transfer or catalyst turnover.[81, 82] Moreover, to compare the turnover numbers of the catalysts in the electrocatalysis, **1b**$(ClO_4)_2$ is 1.8 while [Ru(tpy)(**dpa**)(OH_2)]$(ClO_4)_2$ is 1.2 and **2b**$(ClO_4)_2$ is 0.4 approximately. All these experimental results directly pointed out that an alkyl chain substituted on the 2,2′-dipyridylamine ligand is able to enhance the complex adsorption ability onto the GCE surface, however, the chain length of the alkyl group is critically influence the catalytic activity and efficiency of the complex in the electrochemical water oxidation.

CONCLUSION

The new ruthenium(II)-aqua complexes coordinated with *N*-substituted 2,2′-dipyridylamine ligands (**dppa**, **dpha**, and **dpoa**) were successfully synthesized and their structures were characterized with *X*-ray crystallography. Electrochemical studies showed that the substitution of an alkyl chain to the ligand is able to facilitate the adsorption of the Ru-complex onto the surface of glassy carbon electrode. Moreover, the non-coordinating perchlorate anion was found to take a very crucial role in the promotion of redox $Ru^{III/IV}$ couple in acidic aqueous media. The combination of ligand and anion effects is able to maximize the *in situ* formation and stabilization of Ru^{IV}=O species, which is the active electrocatalyst in water oxidation. The bulk electrolysis demonstrated with an alkyl-tailed [Ru(tpy)(**dppa**)(OH_2)]$^{2+}$ complex was able to produce dioxygen (O_2) effectively and the quantity determined was 1.5 times higher than that of [Ru(tpy)(**dpa**)(OH_2)]$^{2+}$ complex with no alkyl chain substituted in the ligand.

ASSOCIATED CONTENT

Supporting Information.

The following files are available free of charge.

^{1}H NMR of **dppa** and **dpha**; ^{1}H NMR of Ru–**dppa** complexes; Synthesis, characterization, and X-ray structure of **3(ClO$_4$)$_2$**. X-ray structural collection and refinement data, and selected bond length and angle of **1a**(ClO_4), **1b**(CF_3SO_3)$_2$, **2a**(ClO_4), **2b**(CF_3SO_3)$_2$ and **3**(ClO_4)$_2$.

Crystallographic data of **1a**(CF_3SO_3) (CIF)

Crystallographic data of **1b**(ClO_4)$_2$ (CIF)

Crystallographic data of **2a**(CF_3SO_3) **(**CIF)

Crystallographic data of **2b**(CF_3SO_3)$_2$ (CIF)

Crystallographic data of **3**(ClO_4)$_2$ (CIF)

AUTHOR INFORMATION

Corresponding Author

E-mail: kwok-yin.wong@polyu.edu.hk

ACKNOWLEDGMENT

This work was supported by the General Research Fund of the Hong Kong Research Grants Council (PolyU 153338/16P), the Innovation and Technology Commission, and The Hong Kong Polytechnic University. KYW acknowledged the support from the Patrick S.C. Poon endowed professorship.

REFERENCES

1. Meyer, T. J.; Huynh, M. H. V.; Thorp, H. H. The Possible Role of Proton-Coupled Electron Transfer (PCET) in Water Oxidation by Photosystem II. *Angew. Chem. Int. Ed.* **2007,** 46, 5284-5304.
2. Shih, C.; Museth, A. K.; Abrahamsson, M.; Blanco-Rodriguez, A. M.; Di Bilio, A. J.; Sudhamsu, J.; Crane, B. R.; Ronayne, K. L.; Towrie, M.; Vlček, A.; Richards, J. H.; Winkler, J. R.; Gray, H. B. Tryptophan-Accelerated Electron Flow Through Proteins. *Science* **2008,** 320, 1760-1762.
3. Migliore, A.; Polizzi, N. F.; Therien, M. J.; Beratan, D. N. Biochemistry and Theory of Proton-Coupled Electron Transfer. *Chem. Rev.* **2014,** 114, 3381-3465.
4. Williamson, H. R.; Dow, B. A.; Davidson, V. L. Mechanisms for control of biological electron transfer reactions. *Bioorg. Chem.* **2014,** 57, 213-221.
5. Zhong, D. Electron transfer mechanisms of DNA repair by photolyase. *Annu Rev Phys Chem* **2015,** 66, 691-715.
6. Barry, B. A. Reaction dynamics and proton coupled electron transfer: Studies of tyrosine-based charge transfer in natural and biomimetic systems. *Biochim. Biophys. Acta* **2015,** 1847, 46-54.
7. Chang, C. J.; Chang, M. C. Y.; Damrauer, N. H.; Nocera, D. G. Proton-coupled electron transfer: a unifying mechanism for biological charge transport, amino acid radical initiation and propagation, and bond making/breaking reactions of water and oxygen. *Biochim. Biophys. Acta* **2004,** 1655, 13-28.
8. Warren, J. J.; Mayer, J. M. Moving Protons and Electrons in Biomimetic Systems. *Biochemistry* **2015,** 54, 1863-1878.
9. Reece, S. Y.; Nocera, D. G. Proton-coupled electron transfer in biology: results from synergistic studies in natural and model systems. *Annu Rev Biochem* **2009,** 78, 673-99.
10. Boussicault, F.; Robert, M. Electron Transfer in DNA and in DNA-Related Biological Processes. Electrochemical Insights. *Chem. Rev.* **2008,** 108, 2622-2645.
11. Weinberg, D. R.; Gagliardi, C. J.; Hull, J. F.; Murphy, C. F.; Kent, C. A.; Westlake, B. C.; Paul, A.; Ess, D. H.; McCafferty, D. G.; Meyer, T. J. Proton-Coupled Electron Transfer. *Chem. Rev.* **2012,** 112, 4016-4093.
12. Koper, M. T. M. Theory of multiple proton-electron transfer reactions and its implications

for electrocatalysis. *Chem. Sci.* **2013,** 4, 2710-2723.

13. Gentry, E. C.; Knowles, R. R. Synthetic Applications of Proton-Coupled Electron Transfer. *Acc. Chem. Res.* **2016,** 49, 1546-1556.
14. Demchenko, A. P.; Tang, K.-C.; Chou, P.-T. Excited-state proton coupled charge transfer modulated by molecular structure and media polarization. *Chem. Soc. Rev.* **2013,** 42, 1379-1408.
15. Hammes-Schiffer, S. Proton-Coupled Electron Transfer: Moving Together and Charging Forward. *J. Am. Chem. Soc.* **2015,** 137, 8860-8871.
16. Tong, L.; Thummel, R. P. Mononuclear ruthenium polypyridine complexes that catalyze water oxidation. *Chem. Sci.* **2016,** 7, 6591-6603.
17. Gagliardi, C. J.; Vannucci, A. K.; Concepcion, J. J.; Chen, Z.; Meyer, T. J. The role of proton coupled electron transfer in water oxidation. *Energy Environ. Sci.* **2012,** 5, 7704-7717.
18. Blakemore, J. D.; Crabtree, R. H.; Brudvig, G. W. Molecular Catalysts for Water Oxidation. *Chem. Rev.* **2015,** 115, 12974-13005.
19. Richard Keene, F. Metal-ion promotion of the oxidative dehydrogenation of coordinated amines and alcohols. *Coord. Chem. Rev.* **1999,** 187, 121-149.
20. Fukuzumi, S.; Kojima, T.; Lee, Y. M.; Nam, W. High-valent metal-oxo complexes generated in catalytic oxidation reactions using water as an oxygen source. *Coord. Chem. Rev.* **2017,** 333, 44-56.
21. Ishizuka, T.; Kotani, H.; Kojima, T. Characteristics and reactivity of ruthenium-oxo complexes. *Dalton Trans.* **2016,** 45, 16727-16750.
22. Fukuzumi, S. Electron transfer and catalysis with high-valent metal-oxo complexes. *Dalton Trans.* **2015,** 44, 6696-6705.
23. Gagliardi, C. J.; Murphy, C. F.; Binstead, R. A.; Thorp, H. H.; Meyer, T. J. Concerted Electron–Proton Transfer (EPT) in the Oxidation of Cysteine. *J. Phys. Chem. C* **2015,** 119, 7028-7038.
24. Norris, M. R.; Concepcion, J. J.; Harrison, D. P.; Binstead, R. A.; Ashford, D. L.; Fang, Z.; Templeton, J. L.; Meyer, T. J. Redox Mediator Effect on Water Oxidation in a Ruthenium-Based Chromophore–Catalyst Assembly. *J. Am. Chem. Soc.* **2013,** 135, 2080-2083.
25. Goyal, P.; Hammes-Schiffer, S. Tuning the Ultrafast Dynamics of Photoinduced Proton-Coupled Electron Transfer in Energy Conversion Processes. *ACS Energy Lett.* **2017,** 2, 512-

519.

26. de Ruiter, J. M.; Purchase, R. L.; Monti, A.; van der Ham, C. J. M.; Gullo, M. P.; Joya, K. S.; D'Angelantonio, M.; Barbieri, A.; Hetterscheid, D. G. H.; de Groot, H. J. M.; Buda, F. Electrochemical and Spectroscopic Study of Mononuclear Ruthenium Water Oxidation Catalysts: A Combined Experimental and Theoretical Investigation. *ACS Catal.* **2016,** 6, 7340-7349.
27. MacLeod, K. C.; McWilliams, S. F.; Mercado, B. Q.; Holland, P. L. Stepwise N-H Bond Formation From N_2-Derived Iron Nitride, Imide and Amide Intermediates to Ammonia. *Chem. Sci.* **2016,** 7, 5736-5746.
28. Shimoyama, Y.; Ishizuka, T.; Kotani, H.; Shiota, Y.; Yoshizawa, K.; Mieda, K.; Ogura, T.; Okajima, T.; Nozawa, S.; Kojima, T. A Ruthenium(III)–Oxyl Complex Bearing Strong Radical Character. *Angew. Chem. Int. Ed.* **2016,** 55, 14041-14045.
29. Lindley, B. M.; Bruch, Q. J.; White, P. S.; Hasanayn, F.; Miller, A. J. M. Ammonia Synthesis from a Pincer Ruthenium Nitride via Metal–Ligand Cooperative Proton-Coupled Electron Transfer. *J. Am. Chem. Soc.* **2017,** 139, 5305-5308.
30. Pannwitz, A.; Prescimone, A.; Wenger, O. S. Ruthenium(II)–Pyridylimidazole Complexes as Photoreductants and PCET Reagents. *Eur. J. Inorg. Chem.* **2017**, 609-615.
31. Concepcion, J. J.; Jurss, J. W.; Brennaman, M. K.; Hoertz, P. G.; Patrocinio, A. O. T.; Murakami Iha, N. Y.; Templeton, J. L.; Meyer, T. J. Making Oxygen with Ruthenium Complexes. *Acc. Chem. Res.* **2009,** 42, 1954-1965.
32. Zeng, Q.; Lewis, F. W.; Harwood, L. M.; Hartl, F. Role of ligands in catalytic water oxidation by mononuclear ruthenium complexes. *Coord. Chem. Rev.* **2015,** 304, 88-101.
33. Wasylenko, D. J.; Palmer, R. D.; Berlinguette, C. P. Homogeneous water oxidation catalysts containing a single metal site. *Chem. Commun.* **2013,** 49, 218-227.
34. Cao, R.; Lai, W.; Du, P. Catalytic water oxidation at single metal sites. *Energy Environ. Sci.* **2012,** 5, 8134-8157.
35. Takeuchi, K. J.; Thompson, M. S.; Pipes, D. W.; Meyer, T. J. Redox and spectral properties of monooxo polypyridyl complexes of ruthenium and osmium in aqueous media. *Inorg. Chem.* **1984,** 23, 1845-1851.
36. Cabaniss, G. E.; Diamantis, A. A.; Murphy, W. R.; Linton, R. W.; Meyer, T. J. Electrocatalysis of proton-coupled electron-transfer reactions at glassy carbon electrodes. *J.*

Am. Chem. Soc. **1985,** 107, 1845-1853.

37. Dobson, J. C.; Meyer, T. J. Redox properties and ligand loss chemistry in aqua/hydroxo/oxo complexes derived from cis- and trans-$[(bpy)_2RuII(OH_2)_2]^{2+}$. *Inorg. Chem.* **1988,** 27, 3283-3291.
38. Lima, E. C.; Fenga, P. G.; Romero, J.; De Giovani, W. F. Electrochemical behaviour of $[Ru(4,4'\text{-}Me_2bpy)_2(PPh_3)(H_2O)](ClO_4)_2$ in homogeneous solution and incorporated into a carbon paste electrode. Application to oxidations of benzylic compounds. *Polyhedron* **1998,** 17, 313-318.
39. Masllorens, E.; Rodríguez, M.; Romero, I.; Roglans, A.; Parella, T.; Benet-Buchholz, J.; Poyatos, M.; Llobet, A. Can the Disproportion of Oxidation State III Be Favored in Ru(II)-OH_2/Ru(IV)=O Systems? *J. Am. Chem. Soc.* **2006,** 128, 5306-5307.
40. Maji, S.; López, I.; Bozoglian, F.; Benet-Buchholz, J.; Llobet, A. Mononuclear Ruthenium–Water Oxidation Catalysts: Discerning between Electronic and Hydrogen-Bonding Effects. *Inorg. Chem.* **2013,** 52, 3591-3593.
41. Vaquer, L.; Miró, P.; Sala, X.; Bozoglian, F.; Masllorens, E.; Benet-Buchholz, J.; Fontrodona, X.; Parella, T.; Romero, I.; Roglans, A.; Rodríguez, M.; Bo, C.; Llobet, A. Understanding Electronic Ligand Perturbation over Successive Metal-Based Redox Potentials in Mononuclear Ruthenium-Aqua Complexes. *ChemPlusChem* **2013,** 78, 235-243.
42. Rodríguez, M.; Romero, I.; Llobet, A.; Deronzier, A.; Biner, M.; Parella, T.; Stoeckli-Evans, H. Synthesis, Structure, and Redox and Catalytic Properties of a New Family of Ruthenium Complexes Containing the Tridentate bpea Ligand. *Inorg. Chem.* **2001,** 40, 4150-4156.
43. Costentin, C. Electrochemical Approach to the Mechanistic Study of Proton-Coupled Electron Transfer. *Chem. Rev.* **2008,** 108, 2145-2179.
44. Moyer, B. A.; Meyer, T. J. Properties of the oxo/aqua system $(bpy)_2(py)RuO^{2+}/(bpy)_2(py)Ru(OH_2)^{2+}$. *Inorg. Chem.* **1981,** 20, 436-444.
45. Lai, Y.-K.; Wong, K.-Y. Electrochemistry of bis(2,2′ -bipyridine)-diammineruthenium(II) complex in aqueous media at edge-plane pyrolytic graphite electrodes. *J. Electroanal. Chem.* **1994,** 374, 255-261.
46. Wong, K.-Y.; Anson, F. C. Attempts to acclerate the rates of oxidation of ruthenium and osmium tetramethylcyclam complexes at graphite and glassy carbon electrodes and within nafion coatings. *J Electroanal Chem Interfacial Electrochem* **1987,** 237, 69-79.

47. Li, F.; Fan, K.; Wang, L.; Daniel, Q.; Duan, L.; Sun, L. Immobilizing Ru(bda) Catalyst on a Photoanode via Electrochemical Polymerization for Light-Driven Water Splitting. *ACS Catal.* **2015,** 5, 3786-3790.
48. Matheu, R.; Francàs, L.; Chernev, P.; Ertem, M. Z.; Batista, V.; Haumann, M.; Sala, X.; Llobet, A. Behavior of the Ru-bda Water Oxidation Catalyst Covalently Anchored on Glassy Carbon Electrodes. *ACS Catal.* **2015,** 5, 3422-3429.
49. Ashford, D. L.; Sherman, B. D.; Binstead, R. A.; Templeton, J. L.; Meyer, T. J. Electro-assembly of a Chromophore–Catalyst Bilayer for Water Oxidation and Photocatalytic Water Splitting. *Angew. Chem. Int. Ed.* **2015,** 54, 4778-4781.
50. Wang, L.; Fan, K.; Daniel, Q.; Duan, L.; Li, F.; Philippe, B.; Rensmo, H.; Chen, H.; Sun, J.; Sun, L. Electrochemical driven water oxidation by molecular catalysts in situ polymerized on the surface of graphite carbon electrode. *Chem. Commun.* **2015,** 51, 7883-7886.
51. Ashford, D. L.; Lapides, A. M.; Vannucci, A. K.; Hanson, K.; Torelli, D. A.; Harrison, D. P.; Templeton, J. L.; Meyer, T. J. Water Oxidation by an Electropolymerized Catalyst on Derivatized Mesoporous Metal Oxide Electrodes. *J. Am. Chem. Soc.* **2014,** 136, 6578-6581.
52. Tong, L.; Gothelid, M.; Sun, L. Oxygen evolution at functionalized carbon surfaces: a strategy for immobilization of molecular water oxidation catalysts. *Chem. Commun.* **2012,** 48, 10025-10027.
53. Li, F.; Zhang, B.; Li, X.; Jiang, Y.; Chen, L.; Li, Y.; Sun, L. Highly Efficient Oxidation of Water by a Molecular Catalyst Immobilized on Carbon Nanotubes. *Angew. Chem. Int. Ed.* **2011,** 50, 12276-12279.
54. Chen, Z.; Concepcion, J. J.; Jurss, J. W.; Meyer, T. J. Single-Site, Catalytic Water Oxidation on Oxide Surfaces. *J. Am. Chem. Soc.* **2009,** 131, 15580-15581.
55. Mola, J.; Mas-Marza, E.; Sala, X.; Romero, I.; Rodríguez, M.; Viñas, C.; Parella, T.; Llobet, A. Ru-Hbpp-Based Water-Oxidation Catalysts Anchored on Conducting Solid Supports. *Angew. Chem. Int. Ed.* **2008,** 47, 5830-5832.
56. Odrobina, J.; Scholz, J.; Pannwitz, A.; Francàs, L.; Dechert, S.; Llobet, A.; Jooss, C.; Meyer, F. Backbone Immobilization of the Bis(bipyridyl)pyrazolate Diruthenium Catalyst for Electrochemical Water Oxidation. *ACS Catal.* **2017,** 7, 2116-2125.
57. Hornstein, B. J.; Dattelbaum, D. M.; Schoonover, J. R.; Meyer, T. J. Reactivity of an Adsorbed Ru(VI)−Oxo Complex: Oxidation of Benzyl Alcohol. *Inorg. Chem.* **2007,** 46,

8139-8145.

58. Dakkach, M.; Fontrodona, X.; Parella, T.; Atlamsani, A.; Romero, I.; Rodriguez, M. Polypyrrole-functionalized ruthenium carbene catalysts as efficient heterogeneous systems for olefin epoxidation. *Dalton Trans.* **2014,** 43, 9916-9923.
59. Sullivan, B. P.; Calvert, J. M.; Meyer, T. J. Cis-trans isomerism in (trpy)(PPh_3)$RuCl_2$. Comparisons between the chemical and physical properties of a cis-trans isomeric pair. *Inorg. Chem.* **1980,** 19, 1404-1407.
60. Mock, C.; Puscasu, I.; Rauterkus, M. J.; Tallen, G.; Wolff, J. E. A.; Krebs, B. Novel Pt(II) anticancer agents and their Pd(II) analogues: syntheses, crystal structures, reactions with nucleobases and cytotoxicities. *Inorg. Chim. Acta* **2001,** 319, 109-116.
61. Rauterkus, M. J.; Fakih, S.; Mock, C.; Puscasu, I.; Krebs, B. Cisplatin analogues with 2,2′-dipyridylamine ligands and their reactions with DNA model nucleobases. *Inorg. Chim. Acta* **2003,** 350, 355-365.
62. Cheung, K.-C.; Guo, P.; So, M.-H.; Zhou, Z.-Y.; Lee, L. Y. S.; Wong, K.-Y. Ruthenium Terpyridine Complexes Containing a Pyrrole-Tagged 2,2′-Dipyridylamine Ligand—Synthesis, Crystal Structure, and Electrochemistry. *Inorg. Chem.* **2012,** 51, 6468-6475.
63. Chanda, N.; Mobin, S. M.; Puranik, V. G.; Datta, A.; Niemeyer, M.; Lahiri, G. K. Stepwise Synthesis of $[Ru(trpy)(L)(X)]^{n+}$ (trpy = 2,2‘:6‘,2‘ ‘-Terpyridine; L = 2,2‘-Dipyridylamine; X = Cl^-, H_2O, NO_2^-, NO^+, O^{2-}). Crystal Structure, Spectral, Electron-Transfer, and Photophysical Aspects. *Inorg. Chem.* **2004,** 43, 1056-1064.
64. Alessandra Gerli; Jan Reedijk, M. T. L., and Anthony L. Speks. Redox Properties and Electrocatalytic Activity of the Oxo/Aqua System
$[Ru(terpy)(bpz)(O)]^{2+}$/$[Ru(terpy)(bpz)(H_2O)]^{2+}$. X-ray Crystal Structure of
$[Ru(terpy)(bpz)Cl]PF_6$.MeCN (terpy = 2,2’,2’’-Terpyridine; bpz = 2,2’-Bipyrazine). *Inorg. Chem.* **1995,** 34, 1836-1843.
65. Catalano, V. J.; Heck, R. A.; Immoos, C. E.; Öhman, A.; Hill, M. G. Steric Modulation of Electrocatalytic Benzyl Alcohol Oxidation by $[Ru(trpy)(R_2dppi)(O)]^{2+}$ Complexes. *Inorg. Chem.* **1998,** 37, 2150-2157.
66. Catalano, V. J.; Heck, R. A.; Öhman, A.; Hill, M. G. Synthesis, characterization, and electrocatalytic oxidation of benzyl alcohol by a pair of geometric isomers of $[Ru(trpy)(4,4′-Me_2dppi)(OH_2)]^{2+}$ where 4,4′-dppi is 3,6-di-(4-methylpyrid-2-yl)pyridazine. *Polyhedron*

2000, 19, 1049-1055.

67. Mondal, B.; Chakraborty, S.; Munshi, P.; Walawalkar, M. G.; KumarLahiri, G. Ruthenium-(II)/-(III) terpyridine complexes incorporating imine functionalities. Synthesis, structure, spectroscopic and electrochemical properties. *J. Chem. Soc., Dalton Trans.* **2000**, 2327-2335.
68. Patra, S.; Sarkar, B.; Ghumaan, S.; Patil, M. P.; Mobin, S. M.; Sunoj, R. B.; Kaim, W.; Lahiri, G. K. Isomeric ruthenium terpyridine complexes $[Ru(trpy)(L)Cl]^{n+}$ containing the unsymmetrically bidentate acceptor L = 3-amino-6-(3,5-dimethylpyrazol-1-yl)-1,2,4,5-tetrazine. Synthesis, structures, electrochemistry, spectroscopy and DFT calculations. *Dalton Trans.* **2005**, 1188-1194.
69. Maji, S.; Sarkar, B.; Patra, M.; Das, A. K.; Mobin, S. M.; Kaim, W.; Lahiri, G. K. Formation, Reactivity, and Photorelease of Metal Bound Nitrosyl in $[Ru(trpy)(L)(NO)]^{n+}$ (trpy = 2,2′:6′,2′′-Terpyridine, L = 2-Phenylimidazo[4,5-f]1,10-phenanthroline). *Inorg. Chem.* **2008,** 47, 3218-3227.
70. Chand Pramanik, N.; Pramanik, K.; Ghosh, P.; Bhattacharya, S. Chemistry of $[Ru(tpy)(pap)(L')]^{n+}$ (tpy = 2,2′,6′,2″-terpyridine; pap = 2-(phenylazo)pyridine; L′ = Cl^-, H_2O, CH_3CN, 4-picoline, N^{3-}; n = 1,2). X-ray crystal structure of $[Ru(tpy)(pap)(CH_3CN)](ClO_4)_2$ and catalytic oxidation of water to dioxygen by $[Ru(tpy)(pap)(H_2O)]^{2+}$. *Polyhedron* **1998,** 17, 1525-1534.
71. Zong, R.; Naud, F.; Segal, C.; Burke, J.; Wu, F.; Thummel, R. Design and Study of Bi[1,8]naphthyridine Ligands as Potential Photooxidation Mediators in Ru(II) Polypyridyl Aquo Complexes. *Inorg. Chem.* **2004,** 43, 6195-6202.
72. Boyer, J. L.; Polyansky, D. E.; Szalda, D. J.; Zong, R.; Thummel, R. P.; Fujita, E. Effects of a Proximal Base on Water Oxidation and Proton Reduction Catalyzed by Geometric Isomers of $[Ru(tpy)(pynap)(OH_2)]^{2+}$. *Angew. Chem. Int. Ed.* **2011,** 50, 12600-12604.
73. Chen, W.; Rein, F. N.; Scott, B. L.; Rocha, R. C. Catalytic Photooxidation of Alcohols by an Unsymmetrical Tetra(pyridyl)pyrazine-Bridged Dinuclear Ru Complex. *Chem. Eur. J.* **2011,** 17, 5595-5604.
74. Yamazaki, H.; Hakamata, T.; Komi, M.; Yagi, M. Stoichiometric Photoisomerization of Mononuclear Ruthenium(II) Monoaquo Complexes Controlling Redox Properties and Water Oxidation Catalysis. *J. Am. Chem. Soc.* **2011,** 133, 8846-8849.
75. Hirahara, M.; Nagai, S.; Takahashi, K.; Saito, K.; Yui, T.; Yagi, M. New Series of Dinuclear

Ruthenium(II) Complexes Synthesized Using Photoisomerization for Efficient Water Oxidation Catalysis. *Inorg. Chem.* **2015,** 54, 7627-7635.

76. Ohzu, S.; Ishizuka, T.; Hirai, Y.; Jiang, H.; Sakaguchi, M.; Ogura, T.; Fukuzumi, S.; Kojima, T. Mechanistic insight into catalytic oxidations of organic compounds by ruthenium(iv)-oxo complexes with pyridylamine ligands. *Chem. Sci.* **2012,** 3, 3421-3431.
77. Sémon, L.; Boehme, C.; Billard, I.; Hennig, C.; Lützenkirchen, K.; Reich, T.; Roßberg, A.; Rossini, I.; Wipff, G. Do Perchlorate and Triflate Anions Bind to the Uranyl Cation in an Acidic Aqueous Medium? A Combined EXAFS and Quantum Mechanical Investigation. *ChemPhysChem* **2001,** 2, 591-598.
78. Wasylenko, D. J.; Ganesamoorthy, C.; Henderson, M. A.; Koivisto, B. D.; Osthoff, H. D.; Berlinguette, C. P. Electronic Modification of the [RuII(tpy)(bpy)(OH_2)]$^{2+}$ Scaffold: Effects on Catalytic Water Oxidation. *J. Am. Chem. Soc.* **2010,** 132, 16094-16106.
79. Yagi, M.; Tajima, S.; Komi, M.; Yamazaki, H. Highly active and tunable catalysts for O_2 evolution from water based on mononuclear ruthenium(ii) monoaquo complexes. *Dalton Trans.* **2011,** 40, 3802-3804.
80. Allen J. Bard, L. R. F. *Electrochemical Methods: Fundamentals and applications*. John Wiely & Sons, Inc: 2001.
81. *Laboratory Techniques in Electroanalytica Chemistry*. Marcel Dekker, Inc: 1996.
82. Wang, J. *Analytical electrochemistry*. John Wiley & Sons: 2006.

Table of Contents Synopsis and Graphic

SYNOPSIS: The electro-generation of Ru^{IV}=O species from the corresponding Ru^{II}-aqua complex can be promoted significantly with 2,2'-dipyridylamine ligand *N*-substituted with an alkyl chain as the coordinating ligand and the redox $Ru^{III/IV}$ couple is further enhanced with perchlorate anion. The results illustrated the importance of both ligand and anion effects to facilitate the *in situ* formation of Ru^{IV}=O species.

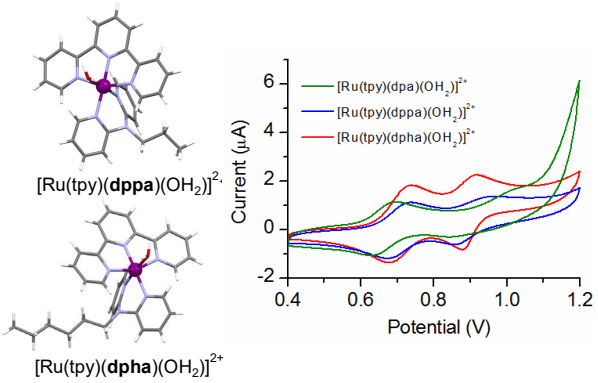

Figure for Table of Contents Only